3

Instabilities of a Parallel Shear Flow

A parallel shear flow is a flow that moves in a single direction, and whose velocity changes in a perpendicular direction, e.g., $\vec{u} = U(z)\hat{e}^{(x)}$. This class of flows includes wakes, jets, boundary layers and shear layers (e.g., Figures 3.2 and 3.3). Parallel shear flows are the simplest class of flows exhibiting the phenomenon of shear instability, in which a fluid is unstable because of spatial variations in its velocity.

Here we will look at shear instability in its most basic form, free of complications due to viscosity, diffusion, buoyancy, or planetary rotation. We'll need to solve an ordinary differential equation, the Rayleigh equation. This can be done analytically for some simple examples (section 3.3), but we'll also make frequent use of the numerical methods introduced in Chapter 1.

Not every parallel shear flow is unstable. We'll prove a simple theorem that often allows us to identify stable cases without solving any equations. Even in an unstable flow, not all types of disturbances grow, so we'll prove two additional results that allow us to distinguish those that do.

Besides developing the needed mathematical theory, we will seek an intuitive understanding of the mechanism of shear instability. This latter goal is considerably more challenging than in the previous case of convection.

3.1 The Perturbation Equations

We assume that

- the flow is inviscid: $\nu = 0$;
- the flow is homogeneous: $\rho = \rho_0$, or $b = 0$;
- Coriolis effects are negligible: $f = 0$.

With these assumptions, the equations of motion (1.17, 1.19) become

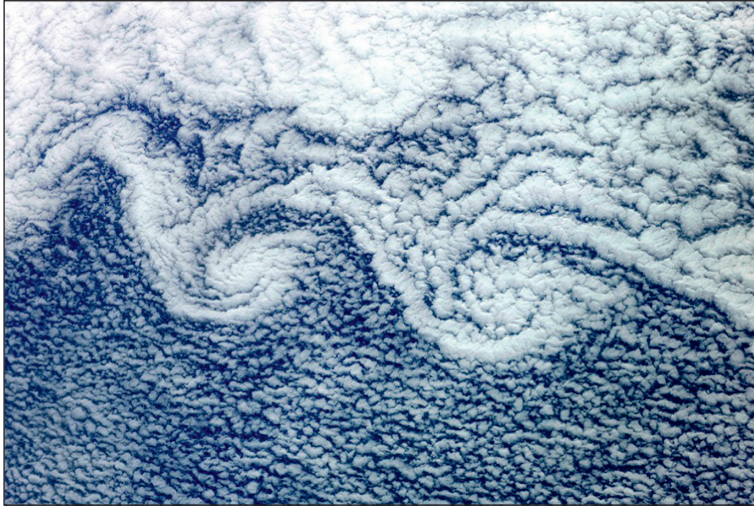$$\vec{\nabla} \cdot \vec{u} = 0 \tag{3.1}$$

53

Figure 3.1 Shear instability at the edge of an altocumulus layer photographed from the International Space Station (NASA).
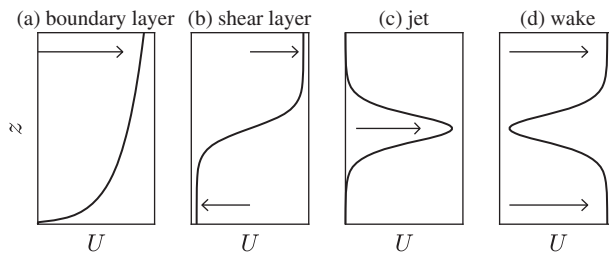

Figure 3.2 Common models of parallel shear flow. (a) Atmospheric or oceanic bottom boundary layer. (b) Shear layer, e.g., Figure 3.3. (c) Jet, e.g., jet stream or Gulf Stream (Figure 1.1). (d) Wake, e.g., island wake in the atmosphere, Figure 3.13.

and

$$\frac{D\vec{u}}{Dt} = -\vec{\nabla}\pi. \tag{3.2}$$

3.1.1 The Equilibrium State

We first seek equilibrium solutions of (3.1, 3.2) having the form of parallel shear flows

$$\vec{u} = U(z)\hat{e}^{(x)}.$$

Note that, while the coordinate z traditionally indicates the vertical direction in geophysical problems, gravity is irrelevant here and z may therefore represent any
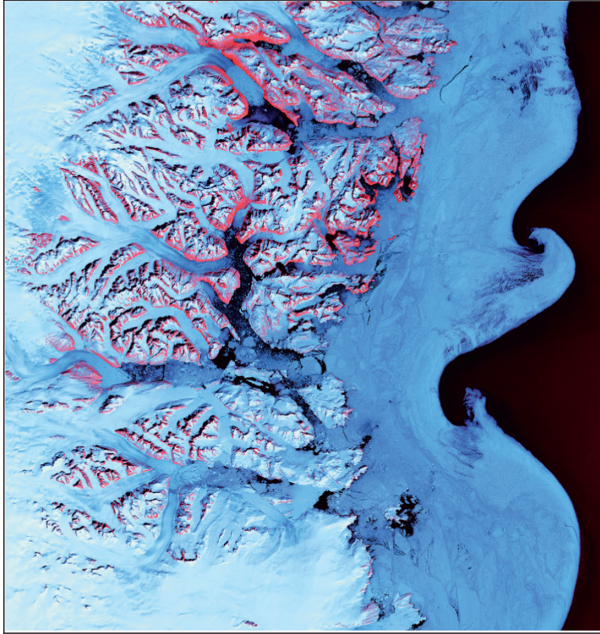
Figure 3.3 Shear instability in a Greenland coastal current made visible by float-ing glacial ice. Landsat 7 satellite photo courtesy United States Geological Survey (hereafter USGS) and NASA.

direction. For example, the instabilities shown in Figures 3.1, 3.3, and 3.13 grow on horizontally sheared flows. In the analysis of those instabilities, z would be directed horizontally across the mean flow.

The continuity equation (3.1) is clearly satisfied:

$$\vec{\nabla} \cdot \vec{u} = \vec{\nabla} \cdot [U(z)\hat{e}^{(x)}] = \frac{\partial}{\partial x} U(z) = 0.$$

The left-hand side of the momentum equation (3.2) is

$$\frac{D\vec{u}}{Dt} = \left[\frac{\partial}{\partial t} + \vec{u} \cdot \vec{\nabla}\right]\vec{u}$$
$$= \left[\frac{\partial}{\partial t} + U(z)\underbrace{\hat{e}^{(x)} \cdot \vec{\nabla}}_{=\partial/\partial x}\right]U(z)\hat{e}^{(x)} = 0,$$

and therefore the right-hand side, $-\vec{\nabla}\pi$ must also be zero. This tells us that any parallel shear flow $U(z)\hat{e}^{(x)}$ is an equilibrium state, provided that the pressure is uniform.

3.1.2 Perturbations from Equilibrium

We next assume that the velocity field consists of a parallel shear flow plus a perturbation:

$$\vec{u} = U(z)\hat{e}^{(x)} + \epsilon\vec{u}'(\vec{x}, t), \tag{3.3}$$

$$\pi = \Pi + \epsilon\pi'(\vec{x}, t), \tag{3.4}$$

where Π is an arbitrary constant as determined in section 3.1.1. Substituting in (3.1), we have

$$\vec{\nabla} \cdot \vec{u} = \vec{\nabla} \cdot \left[U(z)\hat{e}^{(x)} + \epsilon\vec{u}'\right] = \frac{\partial}{\partial x}\left[U(z) + \epsilon u'\right] + \frac{\partial}{\partial y}\epsilon v' + \frac{\partial}{\partial z}\epsilon w' = 0,$$

or

$$\boxed{\vec{\nabla} \cdot \vec{u}' = 0.} \tag{3.5}$$

(In fact, this is always true in an incompressible fluid. The background state must be nondivergent, and therefore the same must be true of the perturbation.)

We next address the momentum equation, (3.2). We begin by substituting (3.3) into the material derivative (1.14):

$$\begin{aligned}
\frac{D}{Dt} &\equiv \frac{\partial}{\partial t} + \vec{u} \cdot \vec{\nabla} \\
&= \frac{\partial}{\partial t} + \left[U(z) + \epsilon u'\right]\frac{\partial}{\partial x} + \epsilon v'\frac{\partial}{\partial y} + \epsilon w'\frac{\partial}{\partial z} \\
&= \frac{\partial}{\partial t} + U(z)\frac{\partial}{\partial x} + \epsilon\vec{u}' \cdot \vec{\nabla}.
\end{aligned} \tag{3.6}$$

Applying this material derivative to $\vec{u}$ gives the left-hand side of (3.2) in perturbation form:

$$\begin{aligned}
\frac{D\vec{u}}{Dt} &= \left(\frac{\partial}{\partial t} + U(z)\frac{\partial}{\partial x} + \epsilon\vec{u}' \cdot \vec{\nabla}\right)\left[U(z)\hat{e}^{(x)} + \epsilon\vec{u}'\right] \\
&= \underbrace{\left(\frac{\partial}{\partial t} + U(z)\frac{\partial}{\partial x}\right)U(z)\hat{e}^{(x)}}_{=0} + \epsilon\underbrace{\vec{u}' \cdot \vec{\nabla}U(z)}_{=w'dU/dz}\hat{e}^{(x)} \\
&\quad + \epsilon\left(\frac{\partial}{\partial t} + U(z)\frac{\partial}{\partial x}\right)\vec{u}' + \underbrace{\epsilon^2[\vec{u}' \cdot \vec{\nabla}]\vec{u}'}_{\approx 0} \\
&= \epsilon w'\frac{dU}{dz}\hat{e}^{(x)} + \epsilon\left(\frac{\partial}{\partial t} + U(z)\frac{\partial}{\partial x}\right)\vec{u}'.
\end{aligned}$$

As usual, the $O(\epsilon^2)$ term is assumed to be negligible. The right-hand side of (3.2) is $-\epsilon\vec{\nabla}\pi'$ since $\vec{\nabla}\Pi = 0$.

Equating the left- and right-hand sides and cancelling the common factor ϵ, the momentum equation for the perturbations is:

$$\boxed{\frac{\partial \vec{u}'}{\partial t} + U(z)\frac{\partial \vec{u}'}{\partial x} + w'\frac{dU}{dz}\hat{e}^{(x)} = -\vec{\nabla}\pi'}.$$

(3.7)

The second term on the left-hand side describes advection of velocity perturbations by the background flow. The third term describes the reverse: the vertical velocity perturbation w' advects the background shear dU/dz to produce perturbations in the x-velocity.

For later convenience, we split into components:

$$\frac{\partial u'}{\partial t} + U\frac{\partial u'}{\partial x} = -\frac{\partial \pi'}{\partial x} - \frac{dU}{dz}w'$$

(3.8)

$$\frac{\partial v'}{\partial t} + U\frac{\partial v'}{\partial x} = -\frac{\partial \pi'}{\partial y}$$

(3.9)

$$\frac{\partial w'}{\partial t} + U\frac{\partial w'}{\partial x} = -\frac{\partial \pi'}{\partial z}.$$

(3.10)

The perturbation equations (3.5) and (3.7) comprise four equations in four unknowns, u', v', w', and π'. As in our previous study of convection, we try to reduce these to a single equation for w'. We begin by deriving the Poisson equation for the pressure perturbation (cf. derivation of 2.16). To do this, we take the divergence of (3.7). The first term is easy:

$$\vec{\nabla} \cdot \frac{\partial \vec{u}'}{\partial t} = \frac{\partial}{\partial t}\vec{\nabla} \cdot \vec{u}' = 0,$$

due to (3.5). The second term is

$$\vec{\nabla} \cdot \left(U(z)\frac{\partial \vec{u}'}{\partial x} \right) = \vec{\nabla}U(z) \cdot \frac{\partial \vec{u}'}{\partial x} + U\frac{\partial}{\partial x}\underbrace{\vec{\nabla} \cdot \vec{u}'}_{=0}$$

$$= U_z\hat{e}^{(z)} \cdot \frac{\partial \vec{u}'}{\partial x}$$

$$= U_z\frac{\partial w'}{\partial x},$$

where the abbreviation U_z has been adopted for the total derivative dU/dz.[1] For the third term we have

$$\vec{\nabla} \cdot \left(w'\frac{dU}{dz}\hat{e}^{(x)} \right) = \frac{\partial}{\partial x}\left(w'\frac{dU}{dz} \right) = U_z\frac{\partial w'}{\partial x}$$

(again!).

---

[1] We will do this frequently to simplify complicated expressions. We must take care, though, because subscripts r and i are also used to denote real and imaginary parts of a complex quantity, and must not be confused with derivatives.

Finally, the right-hand side is

$$-\vec{\nabla} \cdot \vec{\nabla}\pi' = -\nabla^2 \pi.$$

We can now assemble the desired equation:

$$\boxed{\nabla^2 \pi \;=\; -2U_z \frac{\partial w'}{\partial x}.} \tag{3.11}$$

Together with (3.10), this gives us two equations in the two unknowns w' and π'. To eliminate π', we take the Laplacian of (3.10) and substitute:

$$\nabla^2 \frac{\partial w'}{\partial t} + \vec{\nabla} \cdot \vec{\nabla}\left(U \frac{\partial w'}{\partial x}\right) = -\nabla^2 \frac{\partial \pi'}{\partial z},$$

$$\frac{\partial}{\partial t}\nabla^2 w' + \vec{\nabla} \cdot \left(U_z \hat{e}^{(z)} \frac{\partial w'}{\partial x} + U \vec{\nabla}\frac{\partial w'}{\partial x}\right) = -\frac{\partial}{\partial z}\nabla^2 \pi',$$

$$\frac{\partial}{\partial t}\nabla^2 w' + \frac{\partial}{\partial z}\left(U_z \frac{\partial w'}{\partial x}\right) + \vec{\nabla}U \cdot \vec{\nabla}\frac{\partial w'}{\partial x} + U\nabla^2 \frac{\partial w'}{\partial x} = \frac{\partial}{\partial z}\left(2U_z \frac{\partial w'}{\partial x}\right),$$

$$\frac{\partial}{\partial t}\nabla^2 w' + U_z \frac{\partial}{\partial z}\frac{\partial w'}{\partial x} + U\nabla^2 \frac{\partial w'}{\partial x} = U_z \frac{\partial}{\partial z}\frac{\partial w'}{\partial x} + U_{zz}\frac{\partial w'}{\partial x},$$

and finally we have a single equation for w':

$$\boxed{\frac{\partial}{\partial t}\nabla^2 w' + U \frac{\partial}{\partial x}\nabla^2 w' = U_{zz}\frac{\partial w'}{\partial x}.} \tag{3.12}$$

It is instructive to compare this with the corresponding equation for the convective case, (2.17). Again we have the time derivative of $\nabla^2 w'$. But the buoyancy and viscosity terms are now neglected, and instead we have two new terms describing interactions between the perturbation and the parallel shear flow.

3.2 Rayleigh's Equation

3.2.1 Normal Modes in a Shear Flow

As in section 2.2.3, we cannot use the simplest normal mode solution (2.20), because (3.12) does not have constant coefficients; U and U_{zz} are in general functions of z. To allow for this z-dependence, we use the more general normal mode form (2.28), reproduced here for convenience:

$$\boxed{W(\vec{x}, t) = \hat{w}(z)e^{\iota(kx+\ell y)+\sigma t}.} \tag{3.13}$$

As in the convective case, we define the complex function W for analytical convenience; when the time comes to interpret the solution physically, we will retain only the real part:
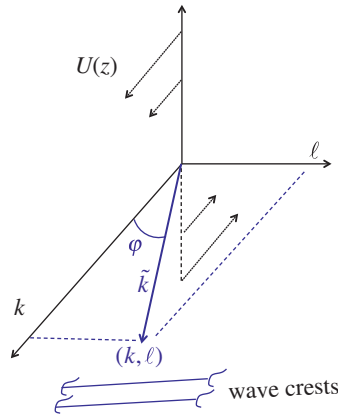
$$w' = W_r.$$

Figure 3.4 Structure of the wave vector for a parallel shear flow, the counterpart of Figure 2.2. The wave vector is horizontal, with components (k, ℓ) and magnitude $\tilde{k}$. The angle of obliquity $\varphi = \cos^{-1} k/\tilde{k}$ is restricted to $-\pi/2 \le \varphi \le \pi/2$.

We note a few more properties of this normal mode form:

- The wave vector $\vec{k} = (k, \ell)$ is directed horizontally as shown in Figure 3.4, with k corresponding to the streamwise (x) direction and ℓ the cross-stream (y) direction. The magnitude of the wavevector is $\tilde{k}$, defined as before: $\tilde{k} = \sqrt{k^2 + \ell^2}$.
- The angle of obliquity, φ, is the angle between the wavevector and the direction of the background flow (x), and is in the range $-\pi/2 \le \varphi \le \pi/2$. Modes are categorized as

  – two-dimensional (2D) if $\varphi = 0$ or, equivalently $\ell = 0$,
  – oblique if $\varphi \ne 0$.

  2D modes have crests perpendicular to the background flow (Figure 3.4).

The normal mode solution (3.13) can also be written in terms of the frequency $\omega = -\iota\sigma$:

$$W = \hat{w}(z)e^{\iota(kx+\ell y - \omega t)}. \tag{3.14}$$

A third alternative is to express the solution in terms of the streamwise phase speed $c = \omega/k$:

$$W = \hat{w}(z)e^{\iota k(x-ct)+\iota\ell y}. \tag{3.15}$$

This is the speed at which a fixed phase of the wave (e.g., a crest or a trough) moves in the x direction (i.e., in a plane $y = $ constant). The phase speed is related to the growth rate by $\sigma = -\iota k c$, or $c = \iota\sigma/k$.

The background flow U is also referred to as the mean flow. Averaging a perturbation of the form (3.13), (3.14), or (3.15) over an integer number of wavelengths in x, y, or both gives zero. Therefore $\bar{u} = \overline{U + u'} = \bar{U} = U$.

3.2.2 Three Forms of Rayleigh's Equation

Returning to the perturbation equation (3.12) and substituting (3.13), the normal mode form written in terms of σ, we obtain a second-order, ordinary differential equation for $\hat{w}(z)$:

$$\sigma \nabla^2 \hat{w} = -\imath k U \nabla^2 \hat{w} + \imath k \frac{d^2 U}{dz^2} \hat{w}, \tag{3.16}$$

where

$$\nabla^2 = \frac{d^2}{dz^2} - \tilde{k}^2. \tag{3.17}$$

This is called Rayleigh's equation after Lord Rayleigh, the inventor of normal modes (Rayleigh, 1880). Together with boundary conditions (often $\hat{w} = 0$ at upper and lower limits of z), these form a differential eigenvalue problem which we will soon convert into an algebraic eigenvalue problem.

Another useful form of Rayleigh's equation results from expanding ∇^2 using (3.17) and rearranging:

$$(\sigma + \imath k U)\left(\frac{d^2}{dz^2} - \tilde{k}^2\right)\hat{w} = \imath k \frac{d^2 U}{dz^2}\hat{w}. \tag{3.18}$$

Rayleigh's equation can also be written in terms of the phase speed. Substituting $\sigma = -\imath k c$ into (3.18), we have

$$\hat{w}_{zz} = \left(\frac{U_{zz}}{U - c} + \tilde{k}^2\right)\hat{w}. \tag{3.19}$$

All three forms of Rayleigh's equation are useful.

3.2.3 Polarization Relations

Normal mode expressions like (3.14) also describe the remaining variables, each with its own vertical structure function: the horizontal velocity components $\hat{u}(z)$ and $\hat{v}(z)$, and the pressure $\hat{\pi}(z)$. Once we know $\hat{w}$, we can calculate the other eigenfunctions. Substituting the normal mode expressions into (3.5), (3.8), and (3.9) gives:

$$\iota(k\hat{u} + \ell\hat{v}) + \hat{w}_z = 0;$$

$$\iota k(U - c)\hat{u} = \iota k\hat{\pi} - U_z\hat{w};$$

$$\iota k(U - c)\hat{v} = -\iota\ell\hat{\pi}.$$

These can be solved algebraically for $\hat{u}$, $\hat{v}$, and $\hat{\pi}$ in terms of $\hat{w}$:

$$\hat{u} = \iota\frac{k}{\tilde{k}^2}\left[\frac{\ell^2}{k^2}\frac{U_z}{U - c}\hat{w} + \hat{w}_z\right], \qquad (3.20)$$

$$\hat{v} = \iota\frac{l}{\tilde{k}^2}\left[-\frac{U_z}{U - c}\hat{w} + \hat{w}_z\right], \qquad (3.21)$$

$$\hat{\pi} = \iota\frac{k}{\tilde{k}^2}\left[U_z\hat{w} - (U - c)\hat{w}_z\right]. \qquad (3.22)$$

Owing to their use in the context of electromagnetic waves, these are referred to as polarization relations.

3.3 Analytical Example: the Piecewise-Linear Shear Layer

The shear layer is a ubiquitous flow shape: it's just a region where the velocity changes from one uniform value to another. Although the mechanism is not as obvious as in the convection case, a shear layer is inherently unstable, and that instability is the main reason naturally occurring flows are almost always turbulent.

In the simplest model of a shear layer, the velocity changes linearly from one value to another. We choose coordinates so that the velocities are $\pm u_0$ and the shear layer boundaries are $z = \pm h$ (Figure 3.5). The velocity profile is then

$$U = u_0\begin{cases} 1, & z \geq h \\ z/h, & -h \leq z \leq h \\ -1, & z \leq -h \end{cases} \qquad (3.23)$$
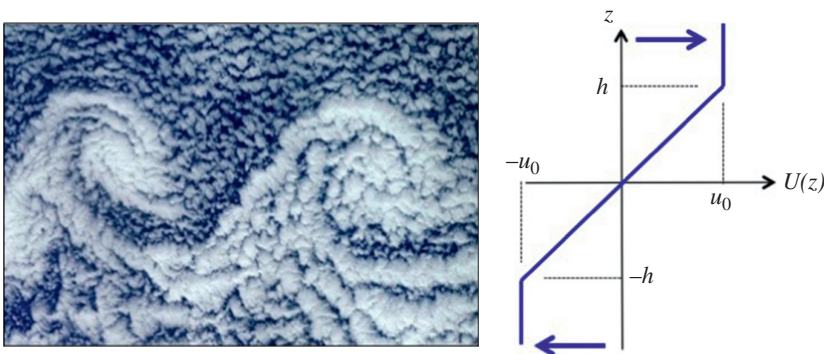

Figure 3.5 Velocity profile (blue) for a linear shear layer with thickness $2h$ and velocity change $2u_0$ (see 3.23). To the left is a disturbance that might grow on such a flow (NASA).

We now use $U(z)$ as input to the Rayleigh equation, which we write in the form (3.19):

$$\hat{w}_{zz} = \left(\frac{U_{zz}}{U - c} + \tilde{k}^2 \right) \hat{w}.$$

Note that U_z is discontinuous at $z = \pm h$, and therefore U_{zz} is infinite at those heights. Specifically

$$U_{zz} = -\frac{u_0}{h} \delta(z + h) + \frac{u_0}{h} \delta(z - h).$$

If the delta function δ is unfamiliar, review section 2.2.4.

3.3.1 Computing the Dispersion Relation

We will solve this problem using the method introduced in section 2.2.4 for convection at an interface, but with two interfaces instead of one. Except at $z = \pm h$, $U_{zz} = 0$, so (3.19) reduces to $\hat{w}_{zz} - \tilde{k}^2 \hat{w} = 0$, and the solution is very simple:

$$\hat{w} = \begin{cases} A_1 e^{\tilde{k}z} + A_2 e^{-\tilde{k}z}, & z \geq h \\ A_3 e^{\tilde{k}z} + A_4 e^{-\tilde{k}z}, & -h \leq z \leq h \\ A_5 e^{\tilde{k}z} + A_6 e^{-\tilde{k}z}, & z \leq -h \end{cases} . \tag{3.24}$$

There are six undetermined constants, so we need six constraints to specify the solution. The first two are obvious: the solution cannot blow up as $z \to \pm\infty$, so

$$A_1 = 0 \quad \text{and} \quad A_6 = 0. \tag{3.25}$$

Another pair of constraints expresses the continuity of $\hat{w}$:

$$[[\hat{w}]]_{\pm h} = 0. \tag{3.26}$$

Applying the constraints (3.25) and (3.26) to (3.24), we have

$$A_2 e^{-\tilde{k}h} = A_3 e^{\tilde{k}h} + A_4 e^{-\tilde{k}h}$$

and

$$A_3 e^{-\tilde{k}h} + A_4 e^{\tilde{k}h} = A_5 e^{-\tilde{k}h}.$$

Substituting these relations into (3.24) and redefining the constants A_3 and A_4 as $B_2 e^{-\tilde{k}h}$ and $B_1 e^{-\tilde{k}h}$, respectively, we can replace (3.24) with the compact form:

$$\boxed{\hat{w}(z) = B_1 e^{-\tilde{k}|z+h|} + B_2 e^{-\tilde{k}|z-h|}.} \tag{3.27}$$

The solution is thus a superposition of two functions, each peaked at one edge of the shear layer, a fact that will be of central importance later. To determine B_1 and B_2 we require jump conditions at $z = h$ and $z = -h$. We will first derive the *general* jump condition for a velocity kink, then apply it to the present case.
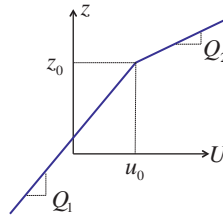
Figure 3.6 Velocity profile (3.28) with a single vorticity interface.

General Jump Condition at a Velocity Kink

Consider an arbitrary piecewise-linear velocity profile with a single kink. The velocity is continuous, but the shear (or vorticity) changes from Q_1 to Q_2 at $z = z_0$:

$$U(z) = u_0 + \begin{cases} Q_2(z - z_0), & z \geq z_0 \\ Q_1(z - z_0), & z \leq z_0 \end{cases} \tag{3.28}$$

The second-derivative is therefore

$$U_{zz} = (Q_2 - Q_1)\,\delta(z - z_0)\,. \tag{3.29}$$

To capture the effect of the kink, we integrate the Rayleigh equation (3.19) over a thin layer from $z_0 - \epsilon$ to $z_0 + \epsilon$, then take the limit as $\epsilon \to 0$:

$$\lim_{\epsilon \to 0} \int_{z_0 - \epsilon}^{z_0 + \epsilon} (\hat{w}_{zz} - \tilde{k}^2 \hat{w})dz = \lim_{\epsilon \to 0} \int_{z_0 - \epsilon}^{z_0 + \epsilon} (Q_2 - Q_1)\,\delta(z - z_0)\,\frac{\hat{w}}{U - c}dz.$$

On the left-hand side, the first term integrates trivially; the result is the change in $\hat{w}_z$ between just above and just below z_0, a difference we write as

$$\lim_{\epsilon \to 0} \hat{w}_z\big|_{z_0 - \epsilon}^{z_0 + \epsilon} \equiv [\![\hat{w}_z]\!]_{z_0}.$$

The second term is $\tilde{k}^2$ times the integral of $\hat{w}$ over a vanishingly small interval. Given that $\hat{w}$ is finite, this integral can only be zero.

On the right-hand side, the combination $\hat{w}(z)/[U(z) - c]$ is integrated with the delta function, picking out its value at $z = z_0$ (see property 6 of the delta function, listed on Figure 2.5).

Finally, noting that $Q_2 - Q_1 \equiv [\![Q]\!]_{z_0}$, the general jump condition is

$$\boxed{[U(z_0) - c]\,[\![\hat{w}_z]\!]_{z_0} = [\![Q]\!]_{z_0}\hat{w}(z_0).} \tag{3.30}$$

Exercise: Review section 2.2.4, the analysis of a density interface. Note the similarities between the solution (2.39) and the present (3.27), and also between the jump conditions (2.41) and (3.30).

Exercise: Convince yourself that, for the shear layer profile (3.23), $[[Q]]_{\pm h} = \mp u_0/h$. Now apply the jump conditions (3.30) to the solution (3.27).

Shear Layer Dispersion Relation

The two equations that determine B_1 and B_2 are:

$$\left[\frac{u_0}{h}e^{-2\tilde{k}h}\right]B_1 + \left[-2\tilde{k}(u_0 - c) + \frac{u_0}{h}\right]B_2 = 0;$$
$$\left[2\tilde{k}(u_0 + c) - \frac{u_0}{h}\right]B_1 + \left[-\frac{u_0}{h}e^{-2\tilde{k}h}\right]B_2 = 0. \qquad (3.31)$$

The set is homogeneous and therefore its determinant must vanish. Solving the resulting equation for c gives the dispersion relation:

$$\boxed{\frac{c^2}{u_0^2} = \left(1 - \frac{1}{2\tilde{k}h}\right)^2 - \frac{e^{-4\tilde{k}h}}{4\tilde{k}^2 h^2}.} \qquad (3.32)$$

3.3.2 Interpreting the Results

Each $\tilde{k}h$ in (3.32) gives two solutions for c. Since the equation involves c^2 and not c, we know that either both values are real or both are imaginary (Figure 3.7a).
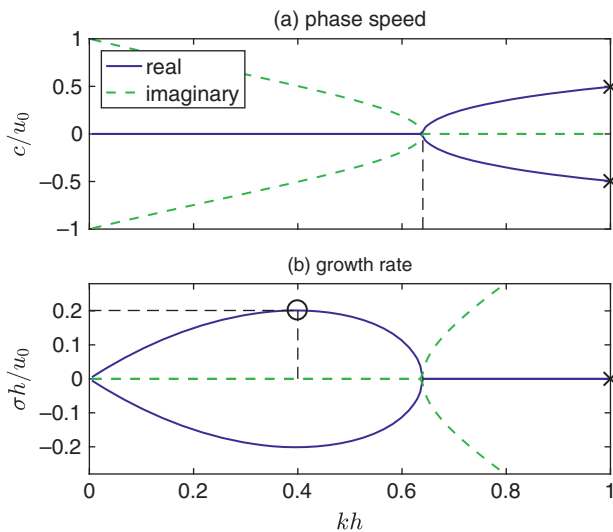

Figure 3.7 Nondimensional phase speed (a) and growth rate (b) for the linear shear layer as given by (3.32, 3.34). Crosses indicate the waves shown on Figure 3.8b,c (red and yellow curves). Circles represent the fastest-growing mode, located at $kh = 0.40$, $\ell h = 0$, $\sigma h/u_0 = 0.20$ (blue curve on Figure 3.8b,c).

Waves

If $c^2 > 0$, c can take either of two real values that are additive inverses. These represent neutrally stable waves with equal but opposite phase speeds. For example, in the limit $\tilde{k}h \to \infty$, (3.32) gives $c/u_0 \to \pm 1$. The positive value gives $B_1 = 0$, i.e., it corresponds to the first term in (3.27),[2] describing a function peaked at $z = +h$. Similarly, $c/u_0 = -1$ gives $B_2 = 0$, corresponding to the peak at $z = -h$.

If $\tilde{k}h$ is finite but sufficiently large, the second term on the right-hand side of (3.32) is negligible (because the exponential function goes to zero faster than any power of its argument) and

$$\frac{c}{u_0} \approx \pm \left(1 - \frac{1}{2\tilde{k}h}\right). \tag{3.33}$$

So, if we start at the right edge of Figure 3.7 and move to lower $\tilde{k}h$, the phase speeds of the oppositely propagating waves converge toward zero. The corresponding eigenfunctions are now combinations of the two terms in (3.27), as shown by the red and yellow curves on Figure 3.8b. Note that each of those functions is dominated by one peak but shows a slight contribution from the other.
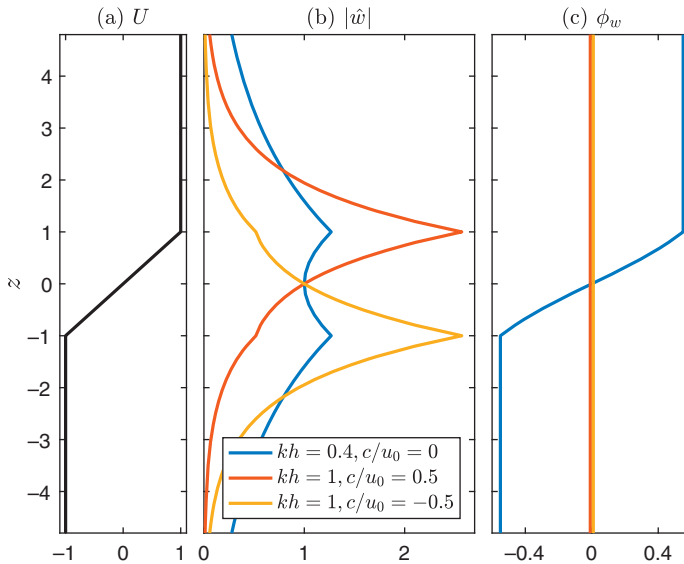

Figure 3.8 Eigenfunction $\hat{w}$ for the piecewise-linear shear layer defined by (3.24) and subsequent constraints. (a) Background velocity profile for reference. (b) Eigenfunction magnitudes for left- and right-going modes with $kh = 1$ (crosses on Figure 3.7) and the fastest-growing mode (circles on Figure 3.7). (c) Eigenfunction phases.

---

[2] To see this, divide (3.31) through by $\tilde{k}$ and set $\tilde{k}h$ to ∞.

Foreshadowing

An interesting interpretation of (3.33) is found by considering the upper and lower edges of the shear layer in isolation. First, suppose that there is no lower edge, i.e., the shear layer extends downward to $-\infty$. In that case, the bounded, continuous solution of the Rayleigh equation is given by the first term of (3.27) alone:

$$\hat{w}(z) = B_2 e^{-\tilde{k}|z-h|}.$$

Applying the jump condition (3.30) leads to the neutral wave solution

$$\frac{c}{u_0} = 1 - \frac{1}{2\tilde{k}h}.$$

Doing the same at the lower edge yields another wave with opposite phase speed:

$$\frac{c}{u_0} = -1 + \frac{1}{2\tilde{k}h}.$$

This pair of solutions is equivalent to (3.33), or to (3.32) without its final term. Therefore, the first term on the right-hand side of (3.32) describes neutral waves that would propagate on each edge of the shear layer if the other edge were not present. The second term, then, can be interpreted as describing the interaction of those two waves. We will have considerably more to say about this in section 3.12.

Instabilities

For $\tilde{k}h < 0.64$ the phase speeds are zero, and the wavelike solutions are replaced by a pair of exponential solutions with imaginary c but real σ (Figure 3.7b). Like the wave solutions, the exponential solutions occur in pairs, now with equal and opposite growth rate.[3] Both the growing mode ($\sigma_r > 0$) and the decaying mode ($\sigma_r < 0$) are classified as stationary – the pattern does not move to the left or the right in a coordinate frame fixed at the center of the shear layer. A mode that is not stationary is called "oscillatory" (cf. discussion in section 2.2.2), because a measurement made at a fixed position oscillates as the disturbance propagates past.

The eigenfunction for the fastest-growing mode (FGM; see section 2.2.2) is shown in Figure 3.8 by the blue curves. In contrast to the wave modes, the eigen-function is symmetric about $z = 0$, having peaks of equal amplitude on the upper and lower edges of the shear layer. Also in contrast to the wave modes, the unstable mode has vertically variable phase (Figure 3.8c). The significance of this will be explored later in section 3.11.4.

---

[3] This is actually a general property of the Rayleigh equation (3.19), as we will see in section 3.4.

To better understand the factors that govern instability, we now rewrite (3.32) in terms of the growth rate by substituting $c = i\sigma/k$, resulting in

$$\sigma = \frac{k}{\tilde{k}} \frac{u_0}{h} f(\tilde{k}h), \quad \text{where } f(x) = \sqrt{\frac{e^{-4x}}{4} - \left(x - \frac{1}{2}\right)^2}. \tag{3.34}$$

This expression for σ has three factors: $k/\tilde{k}$, u_0/h, and $f(\tilde{k}h)$, each of which represents an important influence on growth. We'll discuss these in turn.

(i) Recall that the angle of obliquity φ is the angle between the wave vector and the mean flow (Figure 3.4). For 2D modes (those having $\varphi = 0$), the wave crests are perpendicular to the mean flow. The first factor in (3.34) is

$$\frac{k}{\tilde{k}} = \cos\varphi.$$

This factor tells us that growth is optimized when $\varphi = 0$, i.e., for 2D modes.

(ii) The factor u_0/h tells us that the growth rate is proportional to the shear.

(iii) The function $f(\tilde{k}h)$ is positive in the range $0 < \tilde{k}h < 0.64$ with a single peak $f(0.40) = 0.20$ (Figure 3.7b). This tells us that the shear layer is always unstable, i.e., there is always some value of (k, ℓ) for which $\sigma_r > 0$.

3.3.3 "Rules of Thumb" and the Critical State

Based on these results, we can state four rules of thumb regarding the fastest-growing instability of a piecewise-linear shear layer:

(i) The angle of obliquity is zero, i.e., the wave crests are perpendicular to the mean flow.

(ii) The growth rate is proportional to the shear: $\sigma = 0.20u_0/h$.

(iii) The nondimensional wavenumber is $kh = 0.40$ or, equivalently, the wavelength $\lambda = 2\pi/k = 15.7h$, or about 8 times the thickness of the shear layer.

(iv) The disturbance travels with the speed of the background flow at the center of the shear layer.

The "critical state" for this flow is just $u_0 = 0$. Because there is no mechanism to damp the instability (e.g., viscosity and diffusion, as in the Rayleigh-Benard problem), (3.23) is unstable for any $u_0 \neq 0$.

The piecewise-linear shear layer examined in this section is only one example of the infinite variety of parallel shear flows that are important in nature. In upcoming sections, we will explore analogs of the "rules of thumb" listed above, and more, that apply to *all* parallel shear flows.

3.4 Solution Types for Rayleigh's Equation

We have seen that the dispersion relation (3.32) for the piecewise-linear shear layer (3.23) admits two solution types: real c and oppositely signed pairs of imaginary c. In fact, values of c occur in complex conjugate pairs regardless of the form of $U(z)$. To see this, note that the complex conjugate of (3.19) is

$$\hat{w}_{zz}^* + \left\{ \frac{U_{zz}}{U - c^*} + k^2 \right\} \hat{w}^* = 0$$

(assuming that the wavenumber is real). This is equivalent to (3.19) with c and $\hat{w}$ replaced by their complex conjugates. Therefore, if $[c, \hat{w}]$ is a solution of the Rayleigh equation, then $[c^*, \hat{w}^*]$ is also a solution, and as a result we will obtain either wavelike solutions with c purely real or pairs of solutions in which one grows and the other decays. *In neither case is the flow actually stable*, in the sense that the perturbed flow returns to its equilibrium state. If $c_i \neq 0$, the flow is unstable; if $c_i = 0$, the disturbance oscillates with constant amplitude, i.e., it is neutrally stable.

3.5 Numerical Solution of Rayleigh's Equation

Rayleigh's equation may be solved analytically for certain very simple cases, like the piecewise-linear shear layer of the previous section. In general, though, it must be solved numerically. This requirement is most obvious when $U(z)$ is a velocity profile derived from direct measurements and can therefore be almost arbitrarily complicated (e.g., Figure 3.9). Here we will convert Rayleigh's equation to discretized form, then discuss its numerical solution.

3.5.1 Discretization and the Generalized Eigenvalue Problem

As in section 1.4.2, we place grid points at

$$z_i = i\Delta; \quad i = 0, 1, 2, \ldots, N, N+1,$$

with z_0 and z_{N+1} located at the boundaries. At the interior points $z_1, z_2, \ldots, z_N$ the solution is

$$\hat{w}_i = \hat{w}(z_i); \quad i = 1, 2, \ldots, N.$$

We convert (3.16) into an algebraic equation by discretizing the derivatives. In this case the only derivative is d^2/dz^2, and we discretize it using the second-order derivative matrix $\mathsf{D}^{(2)}$ as defined in (1.13). The derivative matrix may incorporate the impermeable boundary conditions $\hat{w}_0 = \hat{w}_{N+1} = 0$ as in section 1.4.3. Other choices for the boundary conditions will be discussed later (section 3.5.3). With
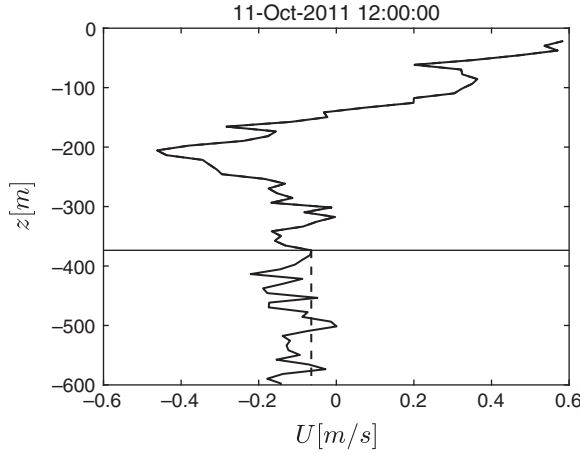
Figure 3.9 Velocity profile measured in the Indian Ocean at the equator at 80.5E longitude (south of Sri Lanka). Total ocean depth is about 4000 m. The horizontal line indicates a plausible depth for a virtual boundary. The fine print: a realistic analysis of this oceanic regime would require inclusion of stratification, viscosity and diffusion (Chapter 6); it is included here only to illustrate a virtual boundary. Data courtesy of Jim Moum, Oregon State University.

the derivative matrix defined, the Laplacian operator (3.17) becomes a matrix that we'll call A:

$$\nabla^2 \ \to \ D^{(2)}_{ij} - \tilde{k}^2 I_{ij} \ = \ A_{ij}. \tag{3.35}$$

The symbol I represents the identity matrix (sometimes called the Kronecker delta).

Next we discretize the velocity profile and its second-derivative to form the vectors $\vec{U}$ and $\vec{U}''$:

$$U_i \ = \ U(z_i); \quad U_i'' \ = \ \left.\frac{d^2U}{dz^2}\right|_{z=z_i}.$$

We can now write the Rayleigh equation in the form (3.16) as

$$\sigma A_{ij}\hat{w}_j \ = \ -\iota k U_i A_{ij}\hat{w}_j \ + \ \iota k U_i'' I_{ij}\hat{w}_j \quad \text{(with no sum on } i\text{)}.$$

Defining a second matrix B as

$$B_{ij} \ = \ -\iota k U_i A_{ij} + \iota k U_i'' I_{ij}, \quad \text{(no sum on } i\text{)}, \tag{3.36}$$

the equation becomes

$$\sigma A_{ij}\hat{w}_j \ = \ B_{ij}\hat{w}_j. \tag{3.37}$$

This is a generalized eigenvalue problem, with eigenvalue σ and eigenvector components $\hat{w}_j$.

3.5.2 Digital Implementation

The eigenvalue problem (3.37) is easily solved using the Matlab function *eig*:

$$[\hat{w}, \sigma] \; = \; \text{eig(B,A).} \tag{3.38}$$

or the equivalent in any other programming environment.

   The most practical approach is to write a subroutine that assembles the matrices A and B and then solves the eigenvalue problem as in (3.38). In due course you will be shown explicitly how to do this, but your understanding will be much deeper if you try it yourself first. Here are some coding hints.

- The routine should have the following inputs: `z, U, k, l`.
- Define the second-derivative matrix `D2` using the subroutine you developed earlier: `ddz2(z)`. For later convenience, design that subroutine using one-sided derivatives for the top and bottom rows. That gives you an easy way to differentiate functions that do not obey boundary conditions, for example: `Uzz=ddz2(z)*U`. When you are ready to incorporate boundary conditions (section 1.4.3), define `D2=ddz2(z)` then replace the top and bottom rows of `D2` according to the boundary conditions you have chosen (more on this in section 3.5.3).
- Define the identity matrix using `I=eye(N)`.
- Compute $\tilde{k}$ as `kt=sqrt(k∧2+l∧2)`. Then compute the Laplacian matrix `A=D2-kt∧2*I`.
- The multiplications in (3.36) are a bit unusual. To compute $U_i A_{ij}$ with no sum on i, each row of A is multiplied by the corresponding element of $\vec{U}$. As a simple example:

$$\vec{U} \cdot \mathsf{A} \; = \; \begin{bmatrix} U_1 A_{11} & U_1 A_{12} & U_1 A_{13} \\ U_2 A_{21} & U_2 A_{22} & U_1 A_{23} \\ U_3 A_{31} & U_3 A_{32} & U_3 A_{33} \end{bmatrix}.$$

This can be written as a standard matrix multiplication:

$$\vec{U} \cdot \mathsf{A} \; = \; \begin{bmatrix} U_1 & 0 & 0 \\ 0 & U_2 & 0 \\ 0 & 0 & U_3 \end{bmatrix} \begin{bmatrix} A_{11} & A_{12} & A_{13} \\ A_{21} & A_{22} & A_{23} \\ A_{31} & A_{32} & A_{33} \end{bmatrix}.$$

The diagonal matrix can be formed using the Matlab function *diag*: `diag(U)*A`. Similarly, $U_i'' I_{ij}$ can be coded as `diag(Uzz)*I`, or just `diag(Uzz)`.

3.5.3 Boundary Conditions: Impermeable and Asymptotic

Rayleigh's equation is often solved with the impermeability condition imposed at horizontal upper and lower boundaries. For a discretized normal mode solution, that boundary condition is just

$$\hat{w}_0 = \hat{w}_{N+1} = 0. \tag{3.39}$$

Approximating the second-derivative using the second-order difference formula

$$\hat{w}_i'' = \frac{\hat{w}_{i-1} - 2\hat{w}_i + \hat{w}_{i+1}}{\Delta^2}, \tag{3.40}$$

the first and last cases are

$$\hat{w}_1'' = \frac{-2\hat{w}_1 + \hat{w}_2}{\Delta^2}; \quad \text{and} \quad \hat{w}_N'' = \frac{\hat{w}_{N-1} - 2\hat{w}_N}{\Delta^2}.$$

The expressions define the top and bottom rows of the second-derivative matrix $\mathsf{D}^{(2)}$.

Finding eigenvalues numerically can be very time-consuming; the time needed to analyze an $N \times N$ matrix is typically proportional to N^2. This can make matrix stability analysis numerically intractable if N exceeds a few hundred. It is therefore important to avoid using large values of N. We next discuss one useful strategy: the application of asymptotic boundary conditions at virtual boundaries. Further strategies are discussed in Chapter 13.

Example: the Ocean Surface Mixed Layer and the Bottom Boundary
In nature, shear instability often occurs in a localized layer far from any boundary, and boundary effects are therefore likely to be negligible. For example, measurements in the upper ocean usually reveal flow features on vertical scales of 10 m or less (e.g., Figure 3.9). The bottom boundary may lie 4000 m or more below this. To include the entire ocean depth in a numerical calculation is impractical. To resolve the shear layer would require $\Delta \sim 1m$ or less, and we would therefore need $N \sim 4000$ grid points, i.e., we would have to calculate the eigenvalues of a 4000×4000 matrix – a very slow process!

One alternative is to place a fictitious lower boundary well below the shear layer. If that boundary is far enough from the shear layer that the vertical velocity perturbation associated with any instability that may emerge is negligible, then the boundary should have negligible effect on the solution. In the ocean example, one could easily imagine that a boundary placed, say, 1000 m below the shear layer would have negligible effect on the results, reducing N to ~ 1000. The assumption can be tested by repeating the calculation with boundaries placed successively farther from shear layer and checking that the results converge.

Another strategy is to assume that the boundary is actually at infinity. In that case, the impermeable boundary condition is replaced by the requirement that the solution remain bounded as $z \to \pm\infty$. This is just what we did in the analytical example of the piecewise-linear shear layer (section 3.3). If U is assumed to approach a constant value far from the layer of interest (e.g., below the horizontal line in Figure 3.9), then the solution to the Rayleigh equation decays with depth in proportion to $e^{\tilde{k}z}$ (cf. 3.24 and 3.25). In a numerical solution, this requirement can be enforced by imposing the boundary condition

$$\hat{w}_z = \tilde{k}\hat{w}$$

at a fictitious boundary chosen reasonably far from the region of interest. This is called an asymptotic boundary condition. It generally has less impact on the solution than an impermeable boundary, and it therefore allows us to use a smaller domain and hence smaller N.

Implementation

Suppose that $U(z)$ varies only in a limited range of z, say $z_B \leq z \leq z_T$, and is constant in the semi-infinite regions $z < z_B$ and $z > z_T$. In either of those outer regions, $U_{zz} = 0$ and the Rayleigh equation (3.19) becomes

$$\hat{w}_{zz} - \tilde{k}^2 \hat{w} = 0,$$

with general solution

$$\hat{w} = A e^{\tilde{k}z} + B e^{-\tilde{k}z}.$$

In the upper region $z > z_T$, the solution is unbounded unless $A = 0$, hence

$$\hat{w} = B e^{-\tilde{k}z}, \quad \text{for } z > z_T. \tag{3.41}$$

We can ensure that our computed solution matches smoothly with (3.41) by imposing the condition

$$\boxed{\hat{w}_z = -\tilde{k}\hat{w} \quad \text{at } z = z_T.} \tag{3.42}$$

Similarly, in the lower layer $z < z_B$, we match to the bounded solution $\hat{w} = A e^{\tilde{k}z}$ by requiring

$$\boxed{\hat{w}_z = \tilde{k}\hat{w} \quad \text{at } z = z_B.} \tag{3.43}$$

To implement asymptotic boundary conditions in a numerical calculation, we approximate (3.42) and (3.43) to second order in Δ by

$$\hat{w}_1' = \frac{\hat{w}_2 - \hat{w}_0}{2\Delta} = \tilde{k}\hat{w}_1 ; \quad \hat{w}_N' = \frac{\hat{w}_{N+1} - \hat{w}_{N-1}}{2\Delta} = -\tilde{k}\hat{w}_N,$$

and therefore

$$\hat{w}_0 = \hat{w}_2 - 2\Delta\tilde{k}\hat{w}_1 \; ; \quad \hat{w}_{N+1} = \hat{w}_{N-1} - 2\Delta\tilde{k}\hat{w}_N. \tag{3.44}$$

Now approximate the second-derivative using the second-order difference formula (3.40) and substitute (3.44) to define the top and bottom rows of the derivative matrix:

$$\mathsf{D}^{(2)} = \frac{1}{\Delta^2} \begin{bmatrix} -2-2\Delta\tilde{k} & 2 & 0 & 0 & \cdots \\ 1 & -2 & 1 & 0 & \cdots \\ 0 & 1 & -2 & 1 & \cdots \\ & & \ddots & & \\ \cdots & 0 & 1 & -2 & 1 \\ \cdots & & & 2 & -2-2\Delta\tilde{k} \end{bmatrix} \tag{3.45}$$

The best way to code the boundary conditions is to begin with a subroutine that calculates the second-derivative matrix $\mathsf{D}^{(2)}$ using one-sided derivatives for the top and bottom rows. After that subroutine is called, replace the top and bottom rows of $\mathsf{D}^{(2)}$ with appropriate values for the boundary conditions you have chosen. In the case of the asymptotic boundary conditions, the Matlab code would look something like this:

```
D2 = ddz2(z);  %2nd derivative matrix with one-sided
derivatives at the boundaries
del = z(2)-z(1);
D2(1,:)=0; ...
D2(1,:)=0; D2(1,1)= -2*(1+del*kt) / del^2; D2(1,2)=
2 / del^2;
D2(N,:)=0; D2(N,N)= -2*(1+del*kt) / del^2; D2(N,N-1)=
2 / del^2.
```

3.6 Shear Scaling

Scaling allows us to investigate the stability of an infinite class of flows all at once. In Chapter 2, we used diffusive scaling, together with the concepts of isomorphic equations and solution algorithms, to arrive at some very general conclusions about convective instability (see section 2.4.1 for a detailed description of diffusive scaling). Here, we will describe a different scaling that is useful for parallel shear flows.

Consider a class of parallel shear flows of the form

$$U(z) = u_0 \, f(z/h), \tag{3.46}$$

where u_0 and h are constants and f is an arbitrary function. We can represent $U(z)$ in the scaled form:

$$U^\star = f(z^\star),$$

where

$$U^\star = \frac{U}{u_0}; \quad z^\star = \frac{z}{h}. \tag{3.47}$$

For example, the piecewise-linear shear layer (3.23) would become

$$U^\star = \begin{cases} 1, & z^\star \geq 1 \\ z^\star, & -1 < z^\star < 1 \\ -1, & z^\star \leq -1 \end{cases} \tag{3.48}$$

Note that this scaling (like the diffusive scaling) yields *nondimensional* forms of U and z.

Now suppose we want to analyze the stability of some class of profiles of the form (3.46) using the Rayleigh equation. We'll use the form (3.18):

$$(\sigma + \iota k U)\left(\frac{d^2}{dz^2} - \tilde{k}^2\right)\hat{w} = \iota k \frac{d^2 U}{dz^2}\hat{w} \tag{3.49}$$

and assume that we have a solution algorithm

$$\sigma = \mathcal{F}(z, U; \, k, \ell). \tag{3.50}$$

Our goal is to express (3.49) in a scaled form. We already have scaled forms for z and U (3.47); we now define scaled versions of the other variables appearing in (3.49) using the same velocity and length scales:

$$\sigma = \sigma^\star \frac{u_0}{h}$$
$$\hat{w} = \hat{w}^\star u_0$$
$$\{\tilde{k}, k, \ell\} = \{\tilde{k}^\star, k^\star, \ell^\star\}/h$$
$$\frac{d}{dz} = \frac{1}{h}\frac{d}{dz^\star}; \quad \nabla^2 = \frac{1}{h^2}\left(\frac{d^2}{dz^{\star 2}} - \tilde{k}^{\star 2}\right). \tag{3.51}$$

Substituting the scaling transformations (3.47) and (3.51) and multiplying by h^3/u_0^2 yields

$$(\sigma^\star + \iota k^\star U^\star)\left(\frac{d^2}{dz^{\star 2}} - \tilde{k}^{\star 2}\right)\hat{w}^\star = \iota\, k^\star \frac{d^2 U^\star}{dz^{\star 2}}\,\hat{w}^\star. \tag{3.52}$$

Comparison of (3.52) and (3.49) shows that (3.52) $\leftrightarrow$ (3.49), and the solution algorithm is therefore the same:

$$\sigma^\star = \mathcal{F}(z^\star, U^\star; \, k^\star, \ell^\star). \tag{3.53}$$

The shear scaling is both a labor-saving device (you can analyze a whole class of flows at once) and a source of insight. For any class of velocity profiles like (3.46),

the fastest-growing mode has a scaled growth rate $\sigma^\star$ and a scaled wave vector $(k^\star, \ell^\star)$, both of which can be calculated using $\mathcal{F}$. For example, in the case of the piecewise-linear shear layer (section 3.3), $\sigma^\star = 0.20$ and $(k^\star, \ell^\star) = (0.40, 0)$.

In dimensional terms, we can draw the following general conclusions from (3.51):

- For every velocity profile of the form (3.46), the fastest growth rate is proportional to the "characteristic shear" u_0/h, with proportionality constant $\sigma^\star$.
- The wavelength $2\pi/\tilde{k}$ of the FGM is proportional to h, with proportionality constant $2\pi/\tilde{k}^\star$.

Admonition: Suppose that the solution algorithm $\mathcal{F}$ is the subroutine described in section 3.5.2. For practical applications, avoid the temptation to write this subroutine in terms of scaled variables. The reason is that you will want to use other scalings in the future. In preparation for that, use the original, dimensional form of the variables, so that the subroutine has the form (3.50). Then, if you want to use shear scaling, call the subroutine using the scaled input variables as in (3.53), and keep in mind that the output will be in scaled form.

Re-dimensionalization

If the solution algorithm described above is used with scaled variables as in (3.53), the results can then be re-dimensionalized to apply to specific situations using (3.47) and (3.51). For example, the piecewise-linear shear layer (3.48) yields instability with scaled growth rate $\sigma^\star = 0.20$ at wavenumber $k^\star = 0.40$ (section 3.9.1). Suppose we want to apply this to a shear layer with half-thickness $h = 2$ m and half velocity change $u_0 = 0.5$ m/s. We would predict a growth rate of $\sigma = \sigma^\star u_0/h = 0.20 \times 0.5 \text{ ms}^{-1}/2 \text{ m} = 0.05 \text{ s}^{-1}$. The e-folding time σ^{-1} is 20 s. The wavelength becomes $2\pi/h = (2\pi/0.40) \times 2 \text{ m} = 31 \text{ m}$.

3.7 Oblique Modes and Squire Transformations

In Chapter 2, we found that the growth rate of convective instability does not depend on k and ℓ individually, but only on their combination $\tilde{k}$. That is *not* the case for parallel shear flows; the direction of the wave vector (k, ℓ) relative to the mean flow matters a lot. Happily, we can draw some general conclusions about this dependence that will spare us from considering every combination of k and ℓ separately.

In the example of the piecewise-linear shear layer (3.23), we found that the fastest-growing mode is 2D. According to (3.34) and the discussion that follows it, if you take any 2D mode and rotate the wave vector to an angle φ from the mean flow, the growth rate is reduced by a factor $\cos\varphi$. We will now show that this

behavior is not peculiar to the linear shear layer; *it is true for any velocity profile*. To demonstrate this powerful result, we introduce Squire transformations.

Recall Rayleigh's equation (3.49, or 3.18):

$$(\sigma + \imath k U)\left(\frac{d^2}{dz^2} - \tilde{k}^2\right)\hat{w} = \imath k U_{zz}\hat{w}, \qquad (3D)$$

and suppose again that we have a solution algorithm

$$\sigma = \mathcal{F}(z, U;\ k, \ell). \qquad (\sigma 3D)$$

The special case of a 2D mode is defined by setting $\ell = 0$ and therefore $\tilde{k} = k$:

$$(\sigma + \imath k U)\left(\frac{d^2}{dz^2} - k^2\right)\hat{w} = \imath k U_{zz}\hat{w}. \qquad (2D)$$

We can find σ for this class of modes by setting $\ell = 0$ in the solution algorithm:

$$\sigma_{2D} = \mathcal{F}(z, U;\ k, 0). \qquad (\sigma 2D)$$

Now, go back to $(3D)$ and substitute the Squire transformations $k = \tilde{k}\cos\varphi$ and $\sigma = \tilde{\sigma}\cos\varphi$. Dividing out the common factor $\cos\varphi$, we have

$$(\tilde{\sigma} + \imath\tilde{k}U)\left(\frac{d^2}{dz^2} - \tilde{k}^2\right)\hat{w} = \imath\tilde{k}U_{zz}\hat{w}. \qquad (\widetilde{3D})$$

The form $(\widetilde{3D})$ is valid for a general 3D mode, but it is also *isomorphic* to the special case $(2D)$:

$$(\widetilde{3D}) \leftrightarrow (2D),\ \text{under } \tilde{\sigma} \to \sigma, \tilde{k} \to k.$$

This means that we can use the same solution algorithm as for the 2D case $(\sigma 2D)$:

$$\tilde{\sigma} = \mathcal{F}(z, U;\ \tilde{k}, 0). \qquad (\sigma\widetilde{3D})$$

or

$$\sigma = \cos\varphi\,\mathcal{F}(z, U;\ \tilde{k}, 0).$$

So, suppose we have a 2D mode with growth rate σ_{2D}. Now rotate the wave vector by an angle φ. The resulting oblique mode will have growth rate $\sigma_{2D}\cos\varphi$. Conversely, *for every oblique mode with wave vector (k, ℓ) and growth rate σ, there is a corresponding 2D mode $(\tilde{k}, 0)$ with higher growth rate $\tilde{\sigma} = \sigma/\cos\varphi$ (Figure 3.10)*. As a consequence, the fastest-growing mode is always 2D.

Like the shear scaling discussed in the previous section, the Squire transformation is a labor saver. If we have some arbitrary flow profile $U(z)$, and we want to know the growth rate for all k, ℓ, we need only calculate the growth rate for the 2D cases, i.e., $\ell = 0$, then for any $\ell \neq 0$ simply multiply the result by $\cos\varphi$. Better still, if we just want to find the FGM, we need only search the 2D cases.
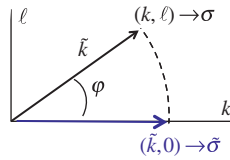
Figure 3.10 Black: wave vector (k, ℓ) of an oblique mode with growth rate σ. Blue: wave vector $(\tilde{k}, 0)$ of the corresponding 2D mode, with growth rate $\tilde{\sigma} = \sigma / \cos \varphi \geq \sigma$.

3.8 Rules of Thumb for a General Shear Instability

Based on sections 3.6 and 3.7, we can now list three rules that apply to the fastest-growing instability of *every* parallel shear flow:

  (i) The fastest-growing mode has wave vector parallel to the mean flow.
 (ii) The growth rate is proportional to u_0 / h.
(iii) The wavelength is proportional to h.

Rules (i–iii) for the piecewise-linear shear layer (section 3.3.3) are a special case of these.

3.9 Numerical Examples

Here we look at two model shear flows (Figure 3.11) for which U is a smooth function of z and the Rayleigh equation must be solved numerically.
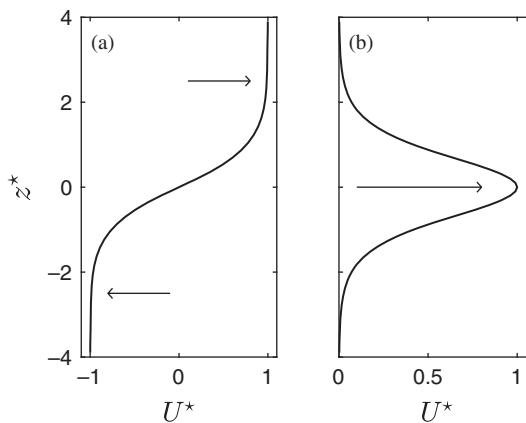

Figure 3.11 Background flow profiles for (a) the hyperbolic tangent shear layer, $U^\star = \tanh z^\star$ and (b) the Bickley jet, $U^\star = \text{sech}^2 z^\star$.
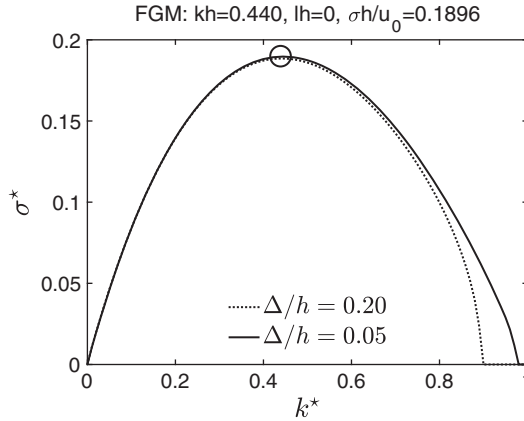
Figure 3.12 Growth rate versus wavenumber for $U^\star = \tanh z^\star$ using two levels of grid resolution. Asymptotic boundary conditions are employed at $z^\star = \pm 4$. In the exact solution, the growth rate drops to zero at $k^\star = 0$ and $k^\star = 1$. Circle shows the fastest-growing mode.

3.9.1 The Hyperbolic Tangent Shear Layer

We consider a smoother version of the piecewise-linear shear layer (Figure 3.11a, cf. Figure 3.5). The velocity profile is modeled by a hyperbolic tangent function $U^\star = \tanh z^\star$. There is no analytical solution, but it can be shown that the growth rate is nonzero for $0 < k^\star < 1$ and $\ell^\star = 0$ (e.g., section 4.4).

The growth rate is computed numerically for $\ell^\star = 0$ and a range of $k^\star$ (Figure 3.12). To test for numerical convergence, the computation is repeated at two values of the grid spacing $\Delta^\star$ (solid and dotted curves). The difference is greatest as $k^\star \to 1$. In the coarsely resolved calculation (dotted), the growth rate drops to zero around $k^\star = 0.9$, in contrast to the exact value $k^\star = 1$. The finely resolved calculation (solid) approximates the exact result more closely. If only the fastest-growing mode is needed, you might decide that the coarser resolution is sufficient.

The result shown in Figure 3.12 is comparable to the piecewise-linear shear layer: the growth rate rises to a peak around $k^\star = 0.44$, and the maximum value is $\sigma^\star = 0.19$. Recall that, for the piecewise-linear shear layer, we got 0.40 and 0.20, respectively (Figure 3.7b). The ratio of wavelength to shear layer thickness for the hyperbolic tangent shear layer is about $(2\pi/0.44)/2 = 7$.

3.9.2 The Bickley Jet

The Bickley jet, $U^\star = \text{sech}^2 z^\star$, is a common model for both jets and wakes (Figure 3.11b). An example is the atmospheric island wake shown in Figure 3.13. The fastest-growing mode has scaled wavenumber $k^\star = 0.9$ and growth rate
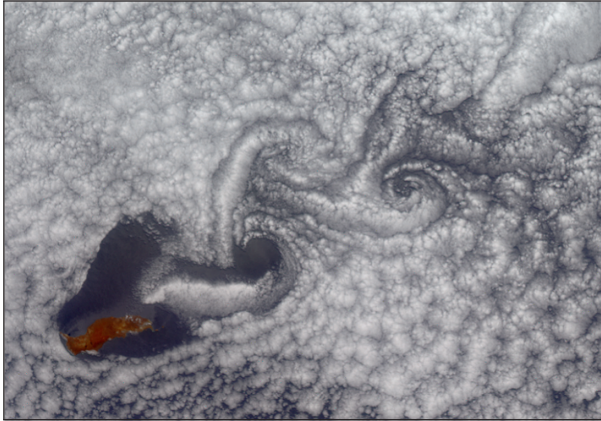
Figure 3.13 Vortex street in the lee of Guadalupe Island in the eastern Pacific. The vortices are formed by the same shear instability that causes a flag to flutter in the wind, the sinuous instability of a plane jet. (NASA)
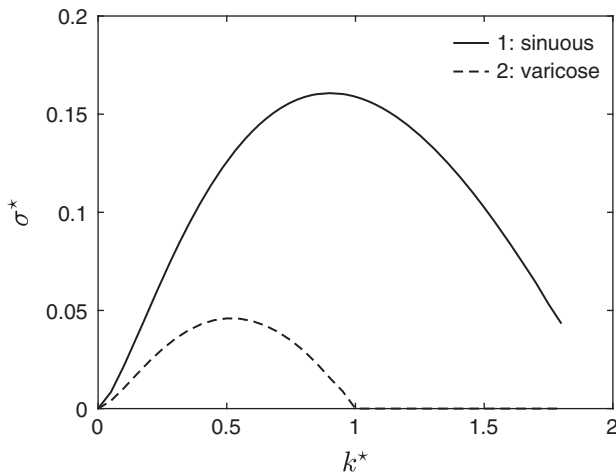

Figure 3.14 Growth rate versus wavenumber for the Bickley jet $U^\star = \operatorname{sech}^2 z^\star$. Asymptotic boundary conditions are employed at $z^\star = \pm 4$. Solid and dashed curves show the sinuous and varicose modes, respectively.

$\sigma^\star = 0.16$ (Figure 3.14). The wavelength is usefully expressed as an aspect ratio, more specifically as a multiple of the jet width $2h$:

$$\frac{\lambda}{2h} = \frac{(2\pi/k^\star)h}{2h} = \frac{\pi}{0.9} = 3.5.$$

This aspect ratio can be compared with Figure 3.13: take the jet width to be the width of the island and λ to be the wavelength of the instability. It is left to the reader to judge whether that ratio compares favorably with our theoretical value.
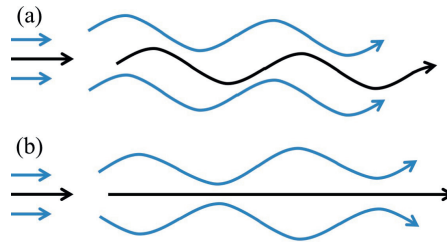
Figure 3.15 Streamlines distinguishing the sinuous (a) and varicose (b) modes of a plane jet. For the sinuous mode (a), the alternating regions of widely separated streamlines correspond to the alternating vortices in the island wake shown in Figure 3.13.

The scaled growth rate 0.16 is quite close to the value for the shear layer, 0.19. This is not an accident; the jet may be thought of as a pair of shear layers set back to back. The instability is then similar to a pair of shear layer instabilities staggered so as to form a vortex street as in Figure 3.13. This jet instability is called the "sinuous mode" (Figure 3.15a).

The dashed curve in Figure 3.14 indicates a second mode of instability called the "varicose mode." This disturbance is also similar to a pair of shear layer instabilities, but in this case the resulting vortices are not staggered but are instead arranged side by side so that the streamlines alternately bulge and constrict (Figure 3.15b). Upper and lower motions oppose one another, so that the varicose mode grows much more slowly than its sinuous counterpart and is seldom seen in naturally occurring flows.

3.10 Perturbation Energetics

The perturbation analyses that we have described so far can tell us whether or not a given flow is unstable and allow us to calculate the length and time scales of the unstable modes. They do not, however, tell us in any intuitive, physical sense how the instability works. To understand instability on this intuitive level, several kinds of auxiliary analysis are helpful. For example, it is almost always enlightening to look at the processes that control the energy of the instability. Here, we will do this for the case of kinetic energy.

A parallel shear flow has kinetic energy. An unstable perturbation grows by accessing that energy and converting it to perturbation kinetic energy. Our goals in this section are to (1) understand the processes by which that energy conversion happens, and (2) learn to quantify those processes via numerical calculations.

3.10.1 Kinetic Energy Evolution in a General Disturbance

For a general physical system, the evolution equation for the kinetic energy is obtained by dotting the velocity vector onto Newton's second law. Here, we

apply this formalism to explore the growth mechanisms for perturbations to a homogeneous, inviscid, parallel shear flow $U(z)$.

The perturbation momentum equation is

$$\frac{\partial \vec{u}'}{\partial t} + U(z)\frac{\partial \vec{u}'}{\partial x} + w'\frac{dU}{dz}\hat{e}^{(x)} = -\vec{\nabla}\pi'$$

[reproducing (3.7)]. Dotting with $\vec{u}'$, we have

$$\vec{u}' \cdot \frac{\partial \vec{u}'}{\partial t} + U(z)\vec{u}' \cdot \frac{\partial \vec{u}'}{\partial x} + w'\frac{dU}{dz}\vec{u}' \cdot \hat{e}^{(x)} = -\vec{u}' \cdot \vec{\nabla}\pi',$$

or

$$\frac{\partial}{\partial t}\left(\frac{\vec{u}' \cdot \vec{u}'}{2}\right) + U(z)\frac{\partial}{\partial x}\left(\frac{\vec{u}' \cdot \vec{u}'}{2}\right) + u'w'\frac{dU}{dz} = -\vec{\nabla} \cdot (\vec{u}'\pi'). \tag{3.54}$$

[To compute the right-hand side of (3.54), we have used both the product rule for the divergence of the vector-scalar product $\vec{u}'\pi'$ and the fact that $\vec{\nabla} \cdot \vec{u}' = 0$.]

Now we apply a horizontal average, to be denoted by an overbar. For this discussion, we assume that there is no dependence on y, so $v' = 0$ and $\partial/\partial y = 0$. (The analysis is easily extended to include y-dependence, the only expense being more complicated algebra; see section 5.9.) Therefore, the horizontal average is taken over x only. Note that $\partial/\partial x$ of any averaged quantity will be zero.

After averaging, the first term on the left-hand side of (3.54) is $\partial K/\partial t$, where

$$K(z, t) = \frac{1}{2}\overline{\vec{u}' \cdot \vec{u}'} = \frac{1}{2}(\overline{u'u'} + \overline{w'w'}) \tag{3.55}$$

is the horizontally averaged perturbation kinetic energy per unit mass. The second term is

$$U\,\frac{\partial K}{\partial x} = 0.$$

The third term does not simplify; it's just

$$\overline{u'w'}\,\frac{dU}{dz}.$$

Finally, the right-hand side becomes

$$-\frac{\partial}{\partial z}\,\overline{w'\pi'}.$$

The result is an equation describing the evolution of the horizontally averaged perturbation kinetic energy:

$$\boxed{\frac{\partial K}{\partial t} = SP - \frac{\partial}{\partial z}EF,} \tag{3.56}$$

where

$$SP = -\frac{dU}{dz}\,\overline{u'w'} \tag{3.57}$$

represents the shear production, the rate at which kinetic energy is transferred from the mean flow to the disturbance, and

$$EF = \overline{w'\pi'} \tag{3.58}$$

represents a vertical flux of kinetic energy. The energy flux transports kinetic energy in the vertical, and its convergence (or divergence) at a given z causes energy to accumulate (or be depleted) at that height.

Equation (3.56) shows that the evolution of perturbation kinetic energy at a given height z is driven by the combination of (1) production by the shear production term and (2) the convergence or divergence of EF. Note that the flux vanishes at the boundaries because $w' = 0$ there. (This is true for impermeable boundaries and also for boundaries at infinity.) Therefore, the vertical integral of $\partial(EF)/\partial z$ over the entire domain is zero, and

$$\frac{d}{dt}\int K\,dz = \int SP\,dz. \tag{3.59}$$

This tells us that only shear production actually creates perturbation kinetic energy; the energy flux just moves it around. The shear production, as defined in (3.57), is revealed as the critical quantity for determining shear instability. We'll take advantage of this fact later.

3.10.2 Kinetic Energy Evolution in a Normal Mode Instability

By plotting the various budget quantities as functions of z, we may gain insight into the processes that drive instability growth. To calculate these quantities, we first substitute the normal mode form (3.14):

$$w' = \{\hat{w}(z)e^{\sigma t + \iota k x}\}_r, \tag{3.60}$$

where the real part has been specified explicitly. Normal mode expressions like (3.60) also describe the remaining variables u' and π'. The vertical structure functions are obtained in terms of $\hat{w}$ by simplifying (3.20) and (3.22) for the special case $\ell = 0$:

$$\hat{u} = \frac{\iota}{k}\frac{d\hat{w}}{dz}, \tag{3.61}$$

$$\hat{\pi} = -(\sigma + \iota kU)\frac{1}{k^2}\frac{d\hat{w}}{dz} + \frac{\iota}{k}\frac{dU}{dz}\hat{w}. \tag{3.62}$$

We're now ready to evaluate the terms in (3.56). We begin with $\overline{u'w'}$. Recall that the real part of any complex quantity a can be written as $(a+a^*)/2$, where the asterisk represents the complex conjugate. Applying this to w' and u' and averaging, we have:

$$\overline{u'w'} = \frac{k}{2\pi} \int\limits_{0}^{2\pi/k} \frac{1}{2}\left\{\hat{u}e^{\sigma t}e^{\iota kx} + \hat{u}^*e^{\sigma *t}e^{-\iota kx}\right\} \times \frac{1}{2}\left\{\hat{w}e^{\sigma t}e^{\iota kx} + \hat{w}^*e^{\sigma *t}e^{-\iota kx}\right\} dx$$

$$= \frac{k}{8\pi} \int\limits_{0}^{2\pi/k} \left\{\hat{u}\hat{w}e^{2\sigma t}e^{2\iota kx} + \hat{u}\hat{w}^*e^{(\sigma+\sigma*)t} + \hat{u}^*\hat{w}e^{(\sigma+\sigma*)t} + \hat{u}^*\hat{w}^*e^{2\sigma *t}e^{-2\iota kx}\right\} dx.$$

In the final integral, the first and last terms integrate to zero. The second and third terms are complex conjugates and do not depend on x, so

$$\overline{u'w'} = \frac{k}{8\pi} \int\limits_{0}^{2\pi/k} \left\{\hat{u}\hat{w}^*e^{(\sigma+\sigma*)t} + \hat{u}^*\hat{w}e^{(\sigma*+\sigma)t}\right\}dx$$

$$= \frac{1}{4}\left\{\hat{u}\hat{w}^*e^{(\sigma+\sigma*)t} + \hat{u}^*\hat{w}e^{(\sigma*+\sigma)t}\right\} = \frac{1}{2}\left\{\hat{u}\hat{w}^*e^{(\sigma+\sigma*)t}\right\}_r$$

$$= \frac{1}{2}\left\{\hat{u}\hat{w}^*\right\}_r e^{2\sigma_r t},$$

We can now generalize this result to give the horizontal average of a product of *any two perturbation quantities*:

$$\boxed{\overline{a'b'} = \frac{1}{2}\left\{\hat{a}\hat{b}^*\right\}_r e^{2\sigma_r t}.} \tag{3.63}$$

This formula may be used in the evaluation of K, SP, or EF. When plotting these quantities, one normally suppresses the time dependence (because it is trivial) by setting $t = 0$. For example, the momentum flux that appears in SP is computed from $\hat{w}$ as:

$$\overline{u'w'} = \frac{1}{2}\left\{\hat{u}\hat{w}^*\right\}_r$$

where the subscript "r" denotes the real part. In Matlab, this expression is easily computed using the functions **conj** and **imag** and your subroutine **ddz** that forms the first-derivative matrix.

In (3.63), note that the time derivative of $\overline{a'b'}$ is just $2\sigma_r \overline{a'b'}$. Applying this result to the perturbation kinetic energy (3.55), the left-hand side of (3.56) becomes $2\sigma_r K$. The kinetic energy equation in normal mode form is therefore
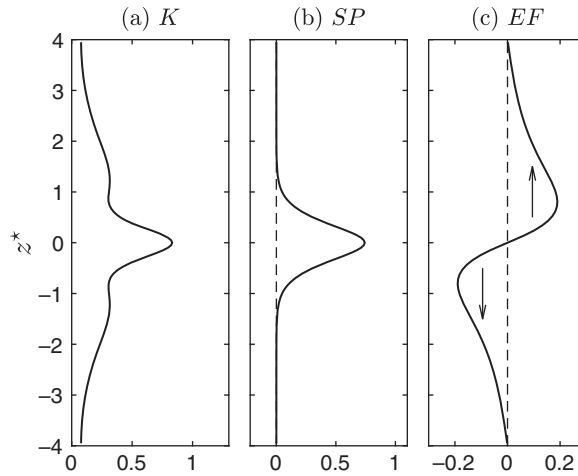
$$\boxed{2\sigma_r K = SP - \frac{d}{dz}EF,} \tag{3.64}$$

Figure 3.16 Perturbation kinetic energy budget (3.56) for the instability of a shear layer $U^\star = \tanh z^\star$. Kinetic energy (a) is extracted from the mean flow within the shear layer via shear production (b), then transported vertically away from the shear layer by the energy flux (c).

where

$$K = \frac{|\hat{u}|^2 + |\hat{v}|^2 + |\hat{w}|^2}{4}, \tag{3.65}$$

$$SP = -\frac{1}{2}\frac{dU}{dz}(\hat{u}^*\hat{w})_r, \tag{3.66}$$

$$EF = \frac{(\hat{w}^*\hat{\pi})_r}{2}. \tag{3.67}$$

Figure 3.16 shows sample results for the instability of a hyperbolic tangent shear layer $U^\star = \tanh z^\star$ (section 3.9.1). Kinetic energy is transferred from the mean flow to the perturbation near the center of the layer by SP (Figure 3.16b), then fluxed outward by EF (Figure 3.16c). Both of these processes are reflected in the shape of the K profile. K is sharply peaked at $z = 0$ because SP is concentrated there, but also shows significant amplitude outside that peak because EF carries some of the energy vertically and deposits it beyond the shear layer.

3.11 Necessary Conditions for Instability

For a particular mode to grow on a particular mean flow, both mode and mean flow must satisfy certain criteria. These are useful to know, because they often allow us to rule out instability without having to do the stability analysis explicitly.

3.11.1 Instability Requires an Inflection Point

We know from (3.59) that growth requires positive net shear production:

$$\int SP\,dz > 0,$$

where the integral covers the whole vertical domain. This means that SP has to be positive for some z. But SP can't be positive for all z, because $\hat{w} = 0$, and therefore $SP = 0$, at the boundaries. Therefore SP must have at least one positive local maximum somewhere in the interior of the flow (e.g., Figure 3.16b). What conditions must the mean flow satisfy for this to be true?

Combining (3.57) and (3.63), we write the shear production as

$$SP = -\frac{1}{2}\,U_z\,\left(\hat{u}\hat{w}^*\right)_r. \tag{3.68}$$

(Don't be confused: The subscript z indicates a derivative, while the subscripts r and i specify the real and imaginary parts, respectively.) Because the fastest-growing mode is invariably two-dimensional (section 3.7), we restrict our attention to 2D modes ($\ell = 0$), in which case

$$\hat{u} = \frac{\iota}{k}\hat{w}_z.$$

With that substitution,

$$\boxed{SP = \frac{U_z}{2k}\,(\hat{w}_z\hat{w}^*)_i.} \tag{3.69}$$

If SP is a maximum, its derivative must be zero. Differentiating, we obtain

$$SP_z = \underbrace{\frac{U_{zz}}{2k}\,(\hat{w}_z\hat{w}^*)_i}_{(1)} + \frac{U_z}{2k}\left[\underbrace{(\hat{w}_{zz}\hat{w}^*)_i}_{(2)} + \underbrace{(\hat{w}_z\hat{w}_z^*)_i}_{(3)}\right].$$

We next simplify the terms (1), (2), and (3) individually.

- (3) is the easiest; it's the imaginary part of an absolute value and is therefore zero.
- (1) can be written as

$$(1) = SP\,\frac{U_{zz}}{U_z}.$$

- (2) is a bit more involved. We begin by writing the Rayleigh equation (3.19) for a 2D disturbance:

$$\hat{w}_{zz} = M\hat{w}, \quad \text{where } M = \frac{U_{zz}}{U - c} + k^2.$$

Now

$$(2) \; = \; (\hat{w}_{zz}\hat{w}^*)_i \; = \; (M\hat{w}\hat{w}^*)_i \; = \; |\hat{w}|^2 M_i.$$

The imaginary part of M is

$$M_i \; = \; \left(\frac{U_{zz}}{U-c} \frac{U-c^*}{U-c^*} + k^2 \right)_i \; = \; \frac{U_{zz}}{|U-c|^2} c_i.$$

Recalling that $c_i = \sigma_r / k$, we can now write (2) as

$$(2) \; = \; |\hat{w}|^2 \frac{U_{zz}}{|U-c|^2} \frac{\sigma_r}{2k^2}.$$

Combining these results we have

$$\begin{aligned} SP_z \; &= \; SP \frac{U_{zz}}{U_z} + |\hat{w}|^2 \frac{U_z U_{zz}}{|U-c|^2} \frac{\sigma_r}{2k^2} \\ &= \; U_z U_{zz} \left(\frac{SP}{U_z^2} + \left| \frac{\hat{w}}{U-c} \right|^2 \frac{\sigma_r}{2k^2} \right). \end{aligned} \tag{3.70}$$

This expression has three factors, at least one of which must be zero if $SP_z = 0$. Because we need a positive maximum of SP, U_z cannot be zero. The term in brackets is positive definite because $SP > 0$ and $\sigma_r > 0$. Therefore, $U_{zz} = 0$. This result includes

Rayleigh's inflection point theorem: *For an inviscid, homogeneous parallel shear flow, a necessary condition for instability is that there exist an inflection point somewhere in the flow.* In addition, the local maximum of SP (where perturbation kinetic energy is produced) coincides with the inflection point.

3.11.2 The Inflection Point Must Be a Shear Maximum

The inflection point specified above (section 3.11.2) may represent a concentration of shear, as in the center of a shear layer, but it may also indicate a layer of reduced shear (compare Figures 3.17a and b). Here we'll show that the former case *may* be unstable, but the latter is definitely *not*.

Note first that the first two factors on the right-hand side of (3.70) can be written as

$$U_z U_{zz} = \frac{1}{2}(U_z^2)_z. \tag{3.71}$$

Therefore, the inflection point is also an extremum of the squared shear: $(U_z^2)_z = 0$, and we can rewrite (3.70) as

$$SP_z \; = \; \frac{1}{2} \left(U_z^2 \right)_z \left(\frac{SP}{U_z^2} + \left| \frac{\hat{w}}{U-c} \right|^2 \frac{\sigma_r}{2k^2} \right).$$
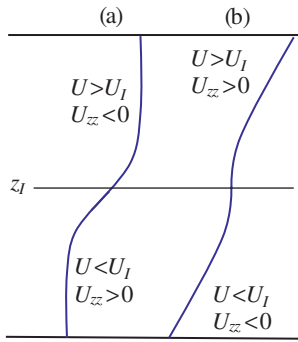
Figure 3.17 Inflectional velocity profiles. $U_I = U(z_I)$ is the velocity at the inflection point z_I. According to the shear production theorem (which includes the Rayleigh and Fjørtoft theorems), (a) may be unstable, whereas (b) is definitely not.

Differentiating, we obtain

$$SP_{zz} = \frac{1}{2} \left(U_z^2 \right)_{zz} \underbrace{\left(\frac{SP}{U_z^2} + \left| \frac{\hat{w}}{U - c} \right|^2 \frac{\sigma_r}{2k^2} \right)}_{>0} + \frac{1}{2} \underbrace{\left(U_z^2 \right)_z}_{=0} \left(\frac{SP}{U_z^2} + \left| \frac{\hat{w}}{U - c} \right|^2 \frac{\sigma_r}{2k^2} \right)_z .$$

Now if our extremum of SP is a maximum, then $SP_{zz} < 0$. Because the quantity in parentheses is positive and the second term is zero,

$$\frac{1}{2} \left(U_z^2 \right)_{zz} < 0.$$

Therefore, the maximum of shear production must also be a maximum of the squared shear.

Alternatively, one can draw the same conclusion in terms of the absolute shear $|U_z|$. Instead of (3.71), start with

$$U_z U_{zz} = |U_z| |U_z|_z,$$

and follow the analysis through in the same way (try it!). The result is that the maximum of shear production must also be a maximum of the *absolute* shear. In visual terms, this means that *the velocity profile around the inflection point must look like Figure 3.17a, not 3.17b*, if SP is to be a maximum. This statement is equivalent to:

Fjørtoft's theorem: *A necessary condition for instability is that $U_{zz}(U - U_I) < 0$ somewhere within the domain of flow, where $U_{zz}(z_I) = 0$, and $U_I = U(z_I)$ is the velocity at the inflection point.*

The standard derivations of the Rayleigh and Fjørtoft theorems are given in the Appendix to this chapter. Also, both results are explained in mechanistic terms in section 3.12.

The results from this and the previous subsection can be summarized as follows:

Shear production theorem: *In an unstable normal mode growing on an inviscid, homogeneous, parallel shear flow, the production of perturbation kinetic energy occurs at a local maximum of the absolute (or squared) shear. If there is no such local maximum, the flow is stable.*

Test your understanding: Is the converse true, i.e., does the presence of a shear maximum guarantee instability?[4]

3.11.3 Instability Requires a Critical Level

In the previous section we found conditions that the *mean flow* must satisfy to be unstable. In this section and the next, we'll look at two conditions that *the perturbation* must satisfy in order to grow.

A glance at Rayleigh's equation in the form (3.19) shows that something special will happen at any height where $U(z) = c$. Since $U - c$ appears in the denominator, such a height is a singularity of (3.19). For unstable modes, c is complex and therefore singularities are located at complex values of z. Near a stability boundary, singularities approach the real z axis. This can become a problem for numerical analysis, since the solution varies rapidly near a singularity and is therefore hard to resolve (Figure 3.18).

On the real z axis, the nearest point to the singularity is that where $U(z) - c_r = 0$. This is the height where the phase speed, relative to the background flow, is zero, i.e., the disturbance is effectively standing still. We call this the critical level.

We now show that every unstable mode must have a critical level. To begin with, write the Rayleigh equation (3.89) with the change of variables

$$\hat{w} = \iota k (U - c) \hat{\eta}. \tag{3.72}$$

Here, $\hat{\eta}$ represents the eigenfunction of the vertical displacement, defined so that $w = D\eta/Dt$. After some algebra (try it, cf. homework problem 9), this leads to

$$[(U - c)^2 \hat{\eta}_z]_z = \tilde{k}^2 (U - c)^2 \hat{\eta}. \tag{3.73}$$

We now multiply by $\hat{\eta}*$ and integrate in the vertical across the domain from z_B to z_T, which may be at $\pm\infty$. We assume that $w' = 0$ at z_B and z_T, which may mean

---

[4] Answer: No. A shear maximum is a necessary, but not a sufficient, condition for instability. A counterexample is derived in homework problem 12 in Appendix A.
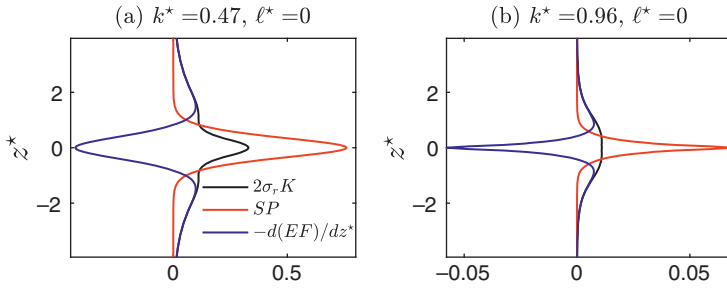
Figure 3.18 Kinetic energy budget terms for two modes of a hyperbolic tangent shear layer $U^\star = \tanh z^\star$. Two cases are compared: (a) far from the stability boundary, and (b) close to the stability boundary. The calculation is done with asymptotic boundary conditions and $\Delta^\star = 0.05$. Case (b) is more difficult to resolve due to the sharp gradients near the critical level $z_c = 0$.

that the boundaries are impermeable or that the disturbance is localized sufficiently to vanish at the boundaries. Integrating the left-hand side by parts and recognizing that $\hat{\eta} = 0$ at the boundaries for all unstable modes,[5] we obtain

$$\int_{z_B}^{z_T} \hat{\eta}^*[(U - c)^2 \hat{\eta}_z]_z dz = -\int_{z_B}^{z_T} \hat{\eta}_z^*(U - c)^2 \hat{\eta}_z dz.$$

Applying the same operations to the right-hand side of (3.73) yields

$$\tilde{k}^2 \int_{z_B}^{z_T} \hat{\eta}^*(U - c)^2 \hat{\eta} dz.$$

Combining, we have

$$\int_{z_B}^{z_T} (U - c)^2 (|\hat{\eta}_z|^2 + \tilde{k}^2 |\hat{\eta}|^2) dz = 0.$$

Now take the imaginary part:

$$c_i \int_{z_B}^{z_T} (U - c_r)(|\hat{\eta}_z|^2 + \tilde{k}^2 |\hat{\eta}|^2) dz = 0.$$

For a growing (or decaying) mode, $c_i \neq 0$, and therefore the integral must be zero. Because the second factor in the integrand is positive definite, the first factor, $U - c_r$, must change sign somewhere in the range of z. In other words:

Critical level theorem: *For an unstable normal mode of a homogeneous, inviscid, parallel shear flow, the phase speed c_r must lie within the range of the background flow.*

---

[5] Referring to (3.72), assume $\hat{w} = 0$ at the boundaries and note that $U - c$ cannot be zero if $c_i \neq 0$.

This result is a corollary of Howard's semicircle theorem, which will be proved in section 4.8.

3.11.4 Shear Production and Phase Tilt

How does one recognize a growing instability observationally? In its early stages, an instability looks like an internal wave, except that it's growing in time. If all you have is a single observation at some point in time, you can't see the growth. A good indicator, then, is the vertical phase structure. At progressively deeper locations, the phase of the wave may remain constant or it may shift in one direction or the other, and that shift can tell us whether the wave is configured properly for growth.

The interpretation of the phase shift depends on the quantity being measured. The easiest choice to handle theoretically is the vertical velocity, so we'll discuss that one here. Suppose that, at some fixed time that we'll call $t = 0$, the vertical velocity has the normal mode form

$$w' = \{\hat{w}(z)e^{\iota k x}\}_r. \tag{3.74}$$

Now let's write the complex amplitude $\hat{w}(z)$ in polar form:

$$\hat{w} = r(z)e^{\iota \phi(z)}. \tag{3.75}$$

Combining (3.74) and (3.75), we have

$$w' = \{r(z)e^{\iota[kx+\phi(z)]}\}_r. \tag{3.76}$$

Any particular phase of the wave (a crest, say, or a trough) is a curve in the $x - z$ plane on which the phase function $\Phi(x, z) = kx + \phi(z)$ has a fixed value (e.g., black dashed line on Figure 3.19). Along such a curve, constancy of $\Phi(x, z)$ requires

$$\Delta\Phi = k\Delta x + \phi_z \Delta z = 0, \quad \text{or} \quad \left(\frac{dz}{dx}\right)_\Phi = -\frac{k}{\phi_z}.$$
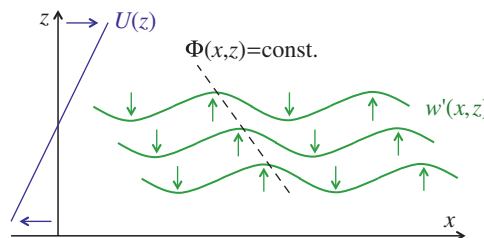

Figure 3.19 Schematic of a vertical velocity field of the form (3.76) with the amplitude r fixed. Note how the phase lines (black) tilt against the sheared background flow (blue).

Now recall that the shear production must be positive for instability. Substituting (3.75) in (3.69),

$$SP = \frac{U_z}{2k}\, (\hat{w}_z \hat{w}^*)_i = \frac{U_z}{2k} \left\{ \left(r_z e^{\iota\phi} + \iota\phi_z r e^{\iota\phi} \right) r e^{-\iota\phi} \right\}_i$$

$$= \frac{U_z}{2k} \{ (r_z + \iota\phi_z r)\, r \}_i = \frac{U_z}{2k}\, r^2 \phi_z = -\frac{U_z}{2}\, \frac{r^2}{(dz/dx)_\Phi}.$$

Therefore $SP > 0$ implies that U_z and $(dz/dx)_\Phi$ have opposite signs. In other words, shear production is positive if and only if the phase lines of w' tilt **against the shear**.

3.11.5 Summary: Conditions for Instability

The following conditions, derived previously in this section, must be satisfied in order for an unstable mode to grow. Conditions (i) and (ii) relate to the mean flow, while conditions (iii) and (iv) relate to the perturbation.

 (i) The mean velocity profile must have an inflection point.
 (ii) The inflection point must represent a maximum (not a minimum) of the absolute shear.
(iii) The mode must have a critical level.
(iv) The phase lines of w' must tilt against the mean shear.

Each of these is a necessary (not a sufficient) condition for growth.

3.12 The Wave Resonance Mechanism of Shear Instability

How does shear instability work? We can solve equations that demonstrate its existence, but is there some intuitive explanation? In the case of convective instability, the answer is obvious: light fluid rises, dense fluid falls. Several explanations have been proposed for shear instability, none as simple as that for convection. Here we will describe a mechanistic picture that has turned out to be quite powerful, not just for shear instability but also for more complex processes such as the baroclinic instability that we will look at later (Chapter 8).

3.12.1 Thought Experiment: Wave Resonance

Consider a piecewise-linear shear layer as in Figure 3.20a, and suppose that the upper edge of the shear layer is somehow deformed to make a sinusoidal wave (upper black curve). Suppose further that this wavelike deformation is held stationary. (Don't be concerned about how this could actually happen; we'll get to that in
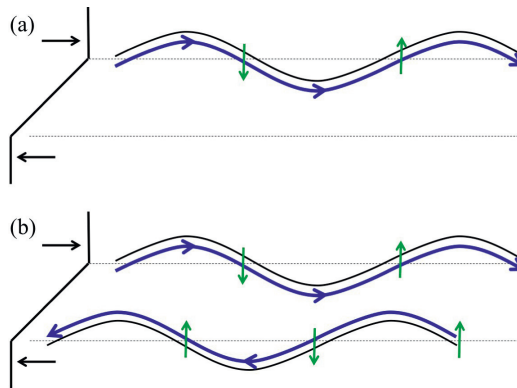
Figure 3.20 Stationary wavelike disturbances in a shear flow. (a) The wavy black curve represents artificially imposed corrugations of the upper edge of a shear layer. The blue arrow shows the path of the flow past the corrugations and green arrows its vertical component. (b) Both edges are corrugated. Mutual amplification results when upward (downward) motions line up with crests (troughs).

the next subsection. For now, just picture inserting a corrugated plastic sheet into the flow.) The flow along the sinusoid is generally from left to right (blue curve), but because of the corrugations it is not purely horizontal; it has a vertical component that alternates in sign, with amplitude greatest at the nodes (green arrows).

Now suppose that the lower edge of the shear layer is also deformed into a stationary sinusoid (Figure 3.20b). The flow along this deformation is from right to left (lower blue curve), again with the vertical component maximized at the nodes.

Finally, suppose that the phase relationship between the two sinusoids is such that the *upward* motions along each sinusoid coincide with the *crests* of the other, and the *downward* motions coincide with the *troughs*, as shown in Figure 3.20b. The result is positive feedback: the bigger the upper disturbance gets, the more it amplifies the lower disturbance, and vice versa. Positive feedback results in exponential growth.

But what kind of waves are these? And how is it that they are able to remain stationary? We'll address the second question first. Two effects combine to allow waves like this to remain stationary. First, Doppler-shifting by the sheared background flow creates the possibility that the phase speeds will be the same (i.e., if each wave propagates *against* the background flow at its own height). The second effect is more subtle.

In Figure 3.21, the solid curves once again show two waves whose phase relationship is optimal for mutual amplification. The solid vertical arrow on the lower wave (marked "1") represents the upward component of the associated motion, extended to emphasize its alignment with the crest of the upper wave.
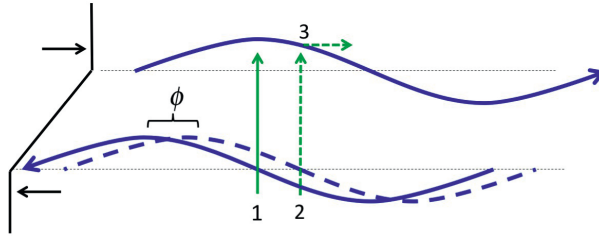
Figure 3.21 Flow along stationary corrugations of the edges of a shear layer as in Figure 3.20. Blue arrows show the path of the flow; green arrows 1 and 2 represent its maximum upward component. The phase relationship shown by the solid blue lines is optimal for mutual amplification, while that with the dashed blue is suboptimal. The interaction accelerates the upper wave to the right (green arrow 3), shifting the phase relationship toward optimal.

Now suppose that the lower wave is shifted to the right by a small amount ϕ (blue dashed curve). The vertical motion associated with the lower wave (arrow 2) is now directed slightly to the *right* of the crest of the upper wave. While this vertical motion still acts to amplify the upper wave, it also tends to shift it to the right (arrow 3), reducing the phase difference ϕ. The same is true of all nodes of both waves. The result is that the upper wave is shifted to the right and the lower wave to the left, reducing ϕ in both cases.

So as long as ϕ is not too large (details in section 3.13.3), the waves tend not only to amplify each other but also to hold each other in place so that amplification can continue. When two waves maintain the same phase velocity, we say that they are phase locked. In the next subsection we will show how waves like this can occur naturally in a shear flow.

3.12.2 Vorticity Waves

We now describe a type of wave whose propagation is driven by a change in vorticity, such as the upper or lower edge of the shear layer in Figure 3.20. Vorticity is a vector field equal to the curl of the velocity. In a two-dimensional flow, vorticity has only a single nonzero component, directed perpendicular to the plane of the flow. That component can be treated as a scalar. For flow in the $x - z$ plane, the scalar vorticity is $q(x, z, t) = u_z - w_x$. For two-dimensional flow in a homogeneous, inviscid fluid,

$$\frac{Dq}{Dt} = 0, \tag{3.77}$$

i.e., a fluid particle's vorticity does not change as it moves through the flow.[6]

---

[6] You can confirm this by writing the equations of motion (1.17, 1.19) for the 2D case:
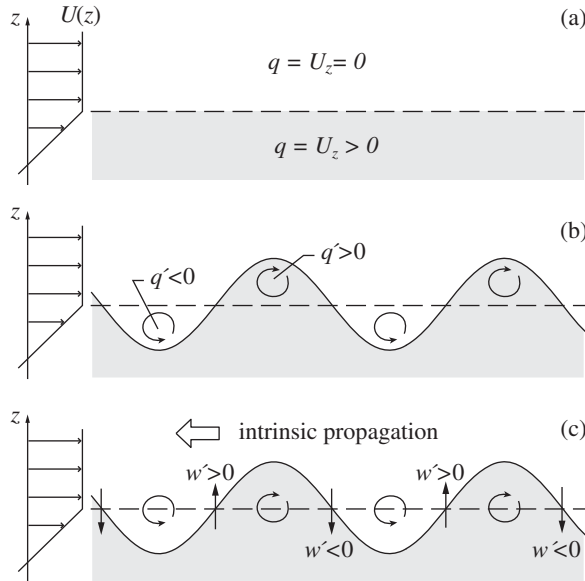
$$u_x + w_z = 0$$

Figure 3.22 Schematic of a vorticity wave propagating on the upper edge of a piecewise-linear shear layer (cf. Figure 3.5). (a) The undisturbed flow, with vorticity positive (clockwise) in the shear layer and zero above. (b) Upward displacements of the interface carry the clockwise vorticity of the shear layer (gray), so the vorticity anomaly in the crests is positive. Downward displacements carry zero vorticity, so the anomaly is negative in the troughs. (c) Counter-rotating vorticity perturbations induce alternately upward and downward motion, causing the pattern to propagate leftward relative to the background flow.

Now, consider the upper edge of a piecewise-linear shear layer (Figure 3.22a, compare with Figure 3.5). Within the undisturbed shear layer, the vorticity is uniform and is given by $q = U_z$. As drawn, U_z is positive, so the sense of the vorticity is clockwise. Outside the shear layer, the vorticity is zero. We will refer to these kinks in the velocity profile, where the vorticity changes abruptly, as vorticity interfaces.

Next let us ask what becomes of a sinusoidal disturbance at the upper edge of the shear layer (Figure 3.22b). Consider a fluid parcel carried upward at a wave crest, i.e., into the region where the vorticity was originally zero. The parcel brings with it

and

$$u_t + u u_x + w u_z = -\pi_x \tag{3.78}$$
$$w_t + u w_x + w w_z = -\pi_z, \tag{3.79}$$

where subscripts indicate partial derivatives. Now differentiate (3.78) and (3.79) with respect to z and x, respectively, and subtract:

$$q_t + u q_x + w q_z = \frac{Dq}{Dt} = 0.$$

its positive vorticity, and the change in vorticity at that location is therefore positive (clockwise circular arrows in Figure 3.22b). Conversely, in regions of downward displacement, the positive ambient vorticity is replaced by zero vorticity from outside the shear layer, so the change is negative. The result is a vorticity perturbation consisting of a row of counter-rotating vortices.

Between each pair of vortices, a region of vertical flow is induced (Figure 3.22c). The direction of this vertical flow alternates, so that the interface moves alternately upward and downward with maximum vertical velocity at its nodes. This causes the whole pattern to move to the left. Note that this leftward motion is opposite, or upstream, relative to the background flow. At the lower edge of the shear layer, the same process produces a rightward propagating wave. Again, propagation is opposite to the mean flow.

Vorticity waves can propagate wherever there is a change in the background vorticity.[7] When the vorticity change takes the form of a sharp kink in the velocity profile, as in this example, the intrinsic propagation is toward the *concave* side of the kink.

So, can vorticity waves at the upper and lower edges of a shear layer be stationary, as we imagined in our thought experiment (section 3.12.1)? The mechanism described above suggests that it is possible, since each wave propagates oppositely to the mean flow at its own elevation. In fact, it can happen rather easily, as will be shown quantitatively in section 3.13.3.

3.12.3 Resonance and the Conditions for Instability

A virtue of the wave resonance model for shear instability is that it allows us to understand, in a visual, mechanistic way, the necessary conditions for instability that we have previously only been able to derive mathematically (section 3.11.5). You will now demonstrate this for yourself by repeating the graphical construction in Figure 3.23 for three other background velocity profiles.

For each of the velocity profiles shown in Figure 3.24, sketch upper and lower waves as follows:

 (i) Draw the *upper wave* at an arbitrary horizontal position.
 (ii) Determine the sense of the vorticity anomaly (clockwise or counterclockwise) in each crest and trough.
(iii) Show the resulting vertical velocity perturbations at the nodes.

---

[7] A well-known example of vorticity waves are the planetary-scale Rossby waves, driven by the gradient in the Coriolis effect between the equator and the poles (Gill, 1982; Pedlosky, 1987). Rossby waves propagate westward relative to the mean flow in the same way that the vorticity waves sketched in Figure 3.22 propagate to the left.
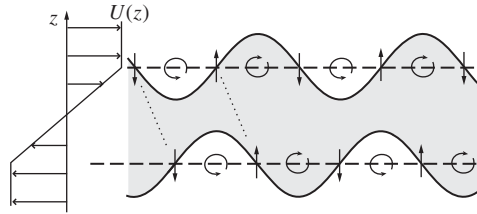
Figure 3.23 Resonant vorticity waves on a shear layer. The mean flow is shown at the left. The upper wave corresponds to Figure 3.22c. Curving arrows represent the vorticity anomalies in the crests and troughs of each wave. Vertical arrows represent the induced vertical motions. Each wave is stationary with respect to the other. Dotted lines are phase lines of w'.
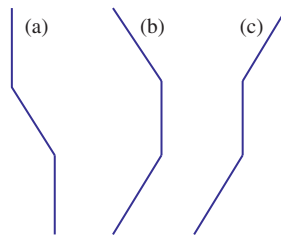

Figure 3.24 Schematics of three piecewise-linear background velocity profiles for use with exercise 3.12.3.

(iv) Indicate the direction of propagation relative to the background flow.
 (v) Sketch the *lower wave* so that its crests and troughs are amplified by the upper wave.
(vi) Now determine the vorticity anomalies, the vertical velocities, and the propagation direction for the lower wave.

   Determine whether the following criteria for resonant growth are satisfied.

 (i) The vertical velocity perturbations of each wave amplify the crests and troughs of the other, creating resonance.
(ii) The propagation directions and mean flow allow for the waves to be stationary relative to each other (i.e., phase-locked), so that the resonance can be sustained over time.

If so, observe how each of the four conditions for growth summarized in section 3.11.5 is satisfied. If not, why not? Identify the condition that is violated.

Results

Admonition: Do not read this until you have tried it yourself!

- For the profile shown in Figure 3.24(a), you should basically reproduce Figure 3.23 with the horizontal direction reversed. Note that the phase lines (lines along which the vertical velocity is constant, i.e., upward arrows or downward arrows) tilt against the shear. If the tilt was opposite, mutual amplification would not occur. Note also that the right-going wave travels against the rightward background flow, and likewise the left-going wave moves against the leftward background flow. If this was not true, phase-locking would be impossible and mutual amplification could not be sustained.
- For (b), you should find that mutual amplification is impossible; if the upper wave amplifies the lower, then the lower wave diminishes the upper, and vice versa. This is because the velocity profile (b) lacks an inflection point (section 3.11.1, Appendix 3.15.1).
- For (c), mutual amplification is possible, but phase-locking is not. The waves always travel in opposite directions. This velocity profile violates the Fjørtoft condition: its inflection point represents a minimum, not a maximum, of the absolute shear (section 3.11.2, Appendix 3.15.2, Figure 3.17b).

If the resonance and phase-locking conditions are satisfied, sketch a line connecting adjacent nodes of the upper and lower waves where the vertical velocity has the same sign, as in Figure 3.23, and note that these lines tilt against the background shear.

So, all four general conditions for instability summarized in section 3.11.5 can be understood intuitively in terms of resonant vorticity waves.

3.13 Quantitative Analysis of Wave Resonance

We'll now take a closer look at the interaction of a pair of vorticity waves propagating on the edges of a shear layer. We begin by deriving the dispersion relation for a single wave (isolated from the influence of the other wave). We'll then look at wave interactions *assuming that this dispersion relation remains valid even when the other wave is present*. This will give us an approximate value for the wavenumber of the fastest-growing mode. Finally, we'll dispense with the assumption about the dispersion relation and see what happens when the waves are allowed to interact.

3.13.1 The Vorticity Wave Dispersion Relation

As a simple model for vorticity wave motion, we solve Rayleigh's equation (3.19) for a velocity profile with a single vorticity interface at $z = z_0$ as shown in Figure 3.6. As in section 3.3, the solution can be written in terms of exponential functions. Requiring that

- $\hat{w}$ decay as $z \to \pm\infty$,
- $\hat{w}$ be continuous across the interface, i.e., $[[\hat{w}]]_{z_0} = 0$,

we obtain

$$\hat{w}(z) = Ae^{-k|z-z_0|}. \tag{3.80}$$

The dispersion relation is found by applying the jump condition (3.30) at the vorticity interface $z = z_0$:

$$\boxed{c = u_0 + \frac{\Delta Q}{2k},} \tag{3.81}$$

where u_0 is the background velocity at the interface and $\Delta Q = Q_2 - Q_1$ is the change in the mean vorticity across the interface. (Exercise: Verify this.) We will call the phase speed relative to the mean velocity, $\Delta Q/(2k)$, the intrinsic phase speed. For the example shown in Figure 3.22, $\Delta Q = -U_z < 0$, so the intrinsic propagation is to the left.

3.13.2 The Isolated Wave Approximation

Now let's consider the full shear layer [(3.23) with waves at both the upper and lower vorticity interfaces (Figure 3.23)]. We assume first that each wave propagates with no influence from the other, so that their phase speeds are given by (3.81). For the upper wave, $\Delta Q = -u_0/h$, so the intrinsic propagation is to the left, opposite to the rightward mean flow. Conversely, the lower wave has $\Delta Q = u_0/h$ and therefore propagates intrinsically to the right against the leftward mean flow. (Remember: the intrinsic vorticity wave propagation is always toward the concave side of the velocity profile.)

The net phase speeds of the upper and lower waves,

$$\frac{c}{u_0} = \pm\left(1 - \frac{1}{2kh}\right), \tag{3.82}$$

are shown by the solid curves on Figure 3.25. (This result was stated without proof in section 3.3.2.) When $kh = 0.5$, the intrinsic phase speed of each wave is exactly opposite to the mean flow, so that its net phase speed is zero.

If the phase relationship is right, the waves reinforce each other as shown in Figure 3.20, and more explicitly in Figure 3.23. Now we'll take it to the next level, refining the theory to account for the fact that the waves do not really propagate independently of each other.
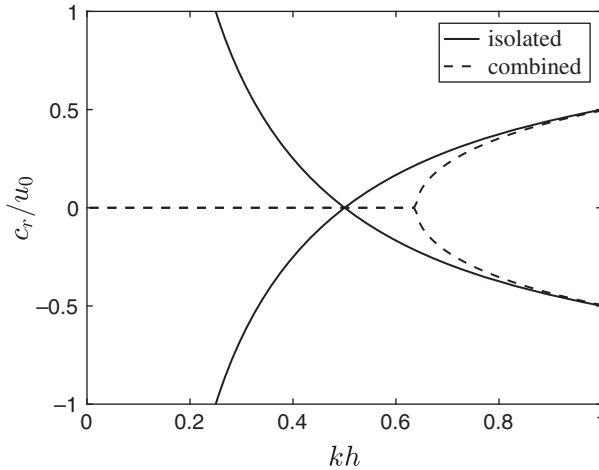
Figure 3.25 Solid: Nondimensional phase speeds of two vorticity waves, isolated from each other, propagating on one or the other edge of a piecewise-linear shear layer, as functions of the nondimensional wavenumber. Dashed: Phase speeds of a pair of counterpropagating stable wave solutions to Rayleigh's equation for a piecewise-linear shear layer, with no assumption of isolation (reproduced from Figure 3.7).

3.13.3 Interaction Effects

With the assumption that the phase speed of each wave is given by (3.81), which means it is unaffected by any other wave (or waves) that may be present, we have identified a single value of kh at which phase-locking occurs, 0.5. But we know that shear instability exists over the whole range $0 < kh < 0.64$ (section 3.3). More-over, the fastest-growing mode has $kh = 0.4$, not 0.5. Could these discrepancies be explained by the influence of each wave on the phase speed of the other?

In section 3.3, we solved the Rayleigh equation for the full velocity profile, without trying to isolate any part from any other part. The phase speed we obtained is shown by the dashed curves on Figure 3.25 (cf. Figure 3.7a). The phase speeds agree well as $kh \to \infty$, but not so well when kh is finite. Recall that the dispersion relation for c is

$$\frac{c^2}{u_0^2} = \underbrace{\left(1 - \frac{1}{2kh}\right)^2}_{isolated\ waves} - \underbrace{\frac{e^{-4kh}}{4k^2h^2}}_{wave\ interaction} . \tag{3.83}$$

[This is just (3.32) simplified by setting ℓ to zero.] We now see that the first term on the right-hand side is what we would get if the two waves were isolated (cf. 3.82), and we can therefore identify the second term as representing the interaction of the two waves, as foreshadowed in section 3.3. That term is negative and therefore

tends to move c toward zero. Moving from large kh (the right-hand side of Figure 3.25) to $kh = 0.64$, the terms in (3.83) come into balance such that the two phase speeds meet at zero. For all smaller values of kh, $c^2 < 0$, meaning that $c_r = 0$ and the waves are phase-locked.

The dependence of the waves' mutual interaction on kh has another important consequence, and that is that the fastest-growing mode is found not at $kh = 0.5$, but rather at $kh = 0.4$ as we discovered in section 3.3. The phase relationship at $kh = 0.4$ is not quite optimal for resonance, but this is compensated for, and then some, by the fact that the waves' amplitude decays more slowly in the vertical at small kh, and hence their ability to amplify each other is greater.

This can all be seen quantitatively by writing the growth rate and the phase speed in terms of the phase relationship between the upper and lower waves. We choose, arbitrarily, to focus on the lower vorticity interface, where the jump condition is

$$(-u_0 - c)[[\hat{w}_z]]_{-h} - \frac{u_0}{h}\hat{w}(-h) = 0, \tag{3.84}$$

giving

$$\frac{c}{u_0} = -1 + \frac{1}{2kh}\left(\frac{B_2}{B_1}e^{-2kh} + 1\right).$$

Let B_1 and B_2 be expressed in polar form $B_1 = A_1 e^{\iota\theta_1}$ and $B_2 = A_2 e^{\iota\theta_2}$. The real constants (A_1, A_2) represent the magnitudes, and (θ_1, θ_2) the phases of the waves at the lower and upper vorticity interfaces. The symmetry of the problem requires that $A_1 = A_2$, hence

$$\frac{c}{u_0} = -1 + \frac{1}{2kh}\left(e^{\iota\Delta\theta - 2kh} + 1\right). \tag{3.85}$$

where we define $\Delta\theta = \theta_2 - \theta_1$. Note that $\Delta\theta = \pi/2 - \phi$, where ϕ is the phase shift defined in Figure 3.20. The real part of (3.85) is

$$\frac{c_r}{u_0} = \underbrace{-1}_{advection} + \overbrace{\frac{1}{2kh}}^{intrinsic} + \underbrace{\cos(\Delta\theta)\frac{e^{-2kh}}{2kh}}_{interaction}. \tag{3.86}$$

The phase speed is composed of three parts: advection by the background profile, the intrinsic propagation speed in isolation, and the change in phase speed due to interaction. When $\Delta\theta = \pi/2$, $\cos\Delta\theta = 0$, and the interaction term is zero. We therefore recover the phase speed of the lower wave in isolation. If that phase speed is zero as in section 3.12.1, then (3.86) gives $kh = 0.5$. But if the waves are allowed to interact, then $\Delta\theta$ is not necessarily $\pi/2$; in fact, $c_r = 0$ requires that

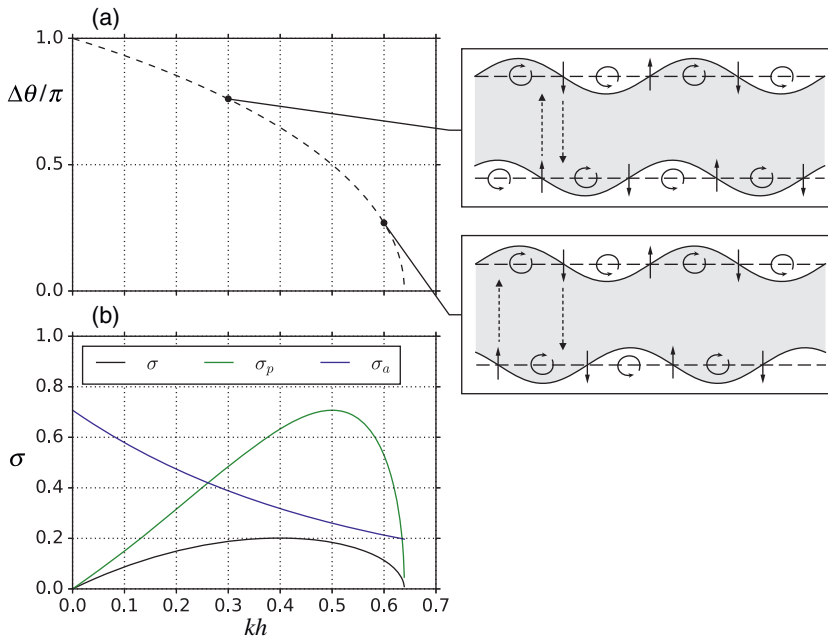$$\cos(\Delta\theta) = e^{2kh}(2kh - 1), \tag{3.87}$$

Figure 3.26 (a) Phase difference between the upper and lower vorticity displacements. The two side panels show the phase configuration of the waves for two values of kh on either side of the crossing point of the isolated dispersion relation. Dashed arrows emphasize the contact point of the maximum vertical velocity with the other wave. (b) Total growth rate (black), represented as a product of two factors: the phase difference ($\sigma_p = \sin(\Delta\theta)/\sqrt{2}$, green) and the amplitude decay ($\sigma_a = e^{-2kh}/\sqrt{2}$, blue), with the factor $1/2$ shared, arbitrarily, between them.

which is plotted in Figure 3.26a. Note that $\Delta\theta$ is less than $\pi/2$ (or $\phi < 0$) when $kh > 1/2$ and greater when $kh < 1/2$.

Now take the imaginary part of (3.85) and solve for the scaled growth rate:

$$\frac{h}{u_0}\sigma = \frac{1}{2}\sin(\Delta\theta)e^{-2kh}. \tag{3.88}$$

Evidently the growth rate is the product of two factors. The first, $\sin(\Delta\theta)$, depends on the phase relationship and is a maximum when $\Delta\theta = \pi/2$ (Figure 3.26b). This is the phase relationship described in section 3.12.1. When $\phi = \pi/2 - \Delta\theta = 0$, the waves are naturally phase-locked without any need for interaction, and are in the optimal phase configuration for growth. The second factor, e^{-2kh}, is the reduction in amplitude of the upper wave at the height of the lower wave (since the vertical distance between them is $2h$), and decreases monotonically with kh. The product of the two (with the constant $1/2$) attains its maximum value 0.20 when $kh = 0.4$, as we found in section 3.3. Therefore, the maximum growth rate occurs not in the
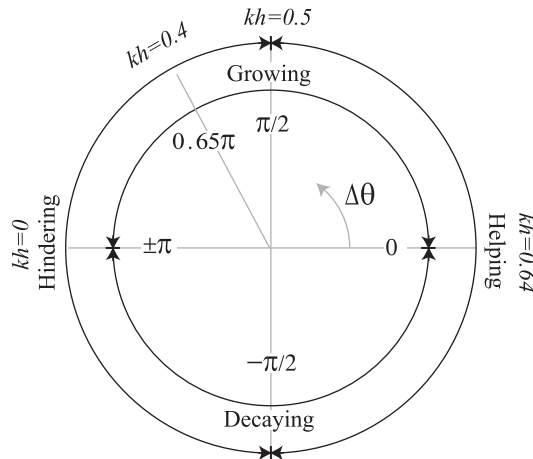
Figure 3.27 Schematic of the effect of wave interactions on the growth and propagation of vorticity waves. Depending on the phase difference, $\Delta\theta$, the waves may cause mutual growth or decay, or they may help or hinder each other's phase propagation. Adapted from Heifetz et al. (2004).

optimal phase relationship $\Delta\theta = \pi/2$, but slightly toward lower kh, where the wave interaction is stronger.

Changes in phase speed and growth rate due to the interaction of two vorticity waves, as quantified in (3.87, 3.88), are diagrammed in Figure 3.27. Depending on the phase difference $\Delta\theta$, we can identify configurations that are optimal for growth ($\Delta\theta = \pi/2$), for decay ($\Delta\theta = -\pi/2$, remembering that every growing mode is accompanied by a decaying mode), and for helping and hindering the intrinsic propagation ($\Delta\theta = 0, \pm\pi$, respectively). In the case of the piecewise shear layer, the bounds of the unstable wavenumber band $kh = 0.64$ and $kh = 0$ coincide with the points of strongest helping/hindering of the phase propagation, $\Delta\theta = 0$ and $\pm\pi$, respectively. A pair of waves with either of these phase relationships will be neutrally stable, but will shift toward either the growth or the decay regime. A pair of waves with $kh = 0.4$ and $\Delta\theta = 0.65\pi$ is optimally configured for growth. Without interaction, the intrinsic propagation term in (3.86) would overcompensate for the advection term, but with $\Delta\theta$ in the "hindering" regime the interaction term brings c_r to zero.

3.14 Summary

Necessary conditions for shear instability in an inviscid, homogeneous fluid:

 (i) The mean velocity profile must have an inflection point.
(ii) The inflection point must represent a maximum (not a minimum) of the absolute shear.

Table 3.1 *Spatial and temporal scales of the fastest-growing mode for two example profiles.*

Name	Formula	$\dfrac{\lambda}{2h}$	$\dfrac{\sigma}{u_0/h}$
hyperbolic tangent shear layer	$U = u_0 \tanh(z/h)$	7	0.19
Bickley jet (sinuous mode)	$U = u_0 \operatorname{sech}^2(z/h)$	3.5	0.16

(iii) The mode must have a critical level.

(iv) The phase lines of w' must tilt against the mean shear.

Characteristics of the fastest-growing mode:

(i) The wave vector is directed parallel to the background flow, i.e., there is no variation in the cross-stream direction.

(ii) If h and u_0 are defined as length and velocity scales characteristic of the mean flow $U(z)$, then the wavelength is proportional to h and the growth rate is proportional to u_0/h. Proportionality constants are given in Table 3.1.

Finally, the resonant interaction of vorticity waves provides an interpretation of the mechanism for shear instability, the Rayleigh and Fjørtoft theorems, and the critical level and phase tilt criteria. In the simplest case, the shear layer, instability is driven by the interaction of two vorticity waves. The fastest-growing mode is that for which the waves are phase-locked and mutual amplification is optimized. In more complex parallel shear flows, instability can be understood in terms of the resonance of multiple vorticity waves.

3.15 Appendix: Classical Proof of the Rayleigh and Fjørtoft Theorems

The shear production theorem proven in section 3.11 is original to this text. It includes the classical theorems of Rayleigh and Fjørtoft, as well as some additional detail about *where* shear instability is expected to occur. In this appendix we give the original proofs of the Rayleigh and Fjørtoft theorems.

We begin by writing the Rayleigh equation in the form (3.19):

$$\hat{w}_{zz} = \frac{U_{zz}}{U - c}\hat{w} + \tilde{k}^2\hat{w}. \tag{3.89}$$

Now multiply by $\hat{w}^*$, the complex conjugate of $\hat{w}$, and integrate:

$$\underbrace{\int \hat{w}^*\hat{w}_{zz}\, dz}_{(1)} = \underbrace{\int \hat{w}^*\frac{U_{zz}}{U - c}\hat{w}\, dz}_{(2)} + \underbrace{\int \hat{w}^*\tilde{k}^2\hat{w}\, dz}_{(3)}. \tag{3.90}$$

The integral is understood to cover the entire vertical domain. We next simplify the terms. Term (3) is the easiest:

$$(3) \;=\; -\tilde{k}^2 \int |\hat{w}|^2 \, dz.$$

Term (1) can be integrated by parts:

$$(1) \;=\; \hat{w}^* \hat{w}_z \Big| - \int \hat{w}_z^* \hat{w}_z \, dz$$

$$=\; 0 - \int |\hat{w}_z|^2 \, dz.$$

The first term vanishes because $\hat{w} = 0$ at the boundaries (either impermeable boundaries or boundaries at infinity). Note that the two terms we've worked on are purely real. Now recall that c is a *complex* phase speed:

$$c = \iota\sigma/k = c_r + \iota c_i;$$

hence, term (2) is complex, and we will split it into real and imaginary parts.

$$(2) \;=\; \int |\hat{w}|^2 \, \frac{U_{zz}}{U - c} \, \frac{U - c^*}{U - c^*} \, dz \;=\; \int \frac{|\hat{w}|^2}{|U - c|^2} \, U_{zz}(U - c_r + \iota c_i) \, dz.$$

Reassembling (3.90) and rearranging, we have

$$\int \frac{|\hat{w}|^2}{|U - c|^2} \, U_{zz}(U - c_r + \iota c_i) \, dz \;=\; -\int |\hat{w}_z|^2 \, dz - \tilde{k}^2 \int |\hat{w}|^2 \, dz. \quad (3.91)$$

3.15.1 Rayleigh's Inflection Point Theorem

Consider the imaginary part of (3.91):

$$c_i \int \frac{|\hat{w}|^2}{|U - c|^2} \, U_{zz} \, dz \;=\; 0. \tag{3.92}$$

For a growing (or decaying) mode, $c_i \neq 0$, and therefore the integral must be zero. Except in the trivial case $\hat{w} = 0$, the integrand must take both positive and negative values in different ranges of z. This requires that U_{zz} change sign at least once in the range of integration, i.e., there must be an inflection point.

3.15.2 Fjørtoft's Theorem

We turn now to the real part of (3.91):

$$\int \frac{|\hat{w}|^2}{|U - c|^2} \, U_{zz}(U - c_r) \, dz \;=\; -\int |\hat{w}|^2 \, dz - \tilde{k}^2 \int |\hat{w}|^2 \, dz. \tag{3.93}$$

If $c_i \neq 0$, then the integral in (3.92) vanishes. We can therefore write:

$$(U_0 - c_r) \int \frac{|\hat{w}|^2}{|U - c|^2} \, U_{zz} \, dz \; = \; 0,$$

where U_0 is an arbitrary, uniform velocity. Subtracting this from (3.93) gives:

$$\int \frac{|\hat{w}|^2}{|U - c|^2} \, U_{zz}(U - U_0) \, dz \; = \; -\int |\hat{w}|^2 \, dz - \tilde{k}^2 \int |\hat{w}|^2 \, dz.$$

Since the right-hand side is negative definite, the integral on the left must be negative, and therefore the integrand must be negative for some z. In other words, the following condition must hold somewhere in the flow:

$$U_{zz}(U - U_0) < 0. \tag{3.94}$$

This is Fjørtoft's theorem.

The geometric meaning of Fjørtoft's theorem is somewhat mysterious due to the arbitrary constant U_0. One way to think of it is that, for some z, U and its second-derivative must have opposite signs. This means that $U(z)$ is wavelike rather than exponential, i.e., it curves back toward zero like a sine or a cosine function. The presence of U_0 guarantees that this is true in any reference frame, as is necessary for any physical law.

A useful choice for U_0 is the velocity at the inflection point, as illustrated in Figure 3.17. We can conclude, for example, that the profile shown in Figure 3.17a may be unstable while that shown in Figure 3.17b is stable.

The form of Fjørtoft's theorem proven in section 3.11.2 may be recovered from (3.94). First, observe that dU_z^2/dz must change sign at an inflection point. Now let $z = z_I$ be an inflection point, and expand the surrounding velocity profile in a Taylor series:

$$U(z) = U(z_I) + U_z(z - z_I) + \dots,$$

where U_z is evaluated at $z = z_I$. Substituting this, the Fjørtoft criterion (3.94) becomes

$$U_{zz} U_z (z - z_I) < 0,$$

or

$$(z - z_I)\frac{1}{2}\frac{dU_z^2}{dz} < 0. \tag{3.95}$$

Since dU_z^2/dz must change sign at z_I, (3.95) requires that dU_z^2/dz be negative just above z_I and positive just below z_I rather than the reverse, i.e., the inflection point must be a maximum (not a minimum) of U_z^2.

3.16 Further Reading

Holmboe (1962), Baines and Mitsudera (1994), and Carpenter et al. (2013) give detailed discussions of shear instability via wave interactions. Heifetz et al. (1999) calculates the fastest-growing mode of a shear layer explicitly using the wave-interaction mechanism.

The original proofs of the Rayleigh and Fjørtoft theorems were published in Rayleigh (1880) and Fjortoft (1950), respectively.